Fidelity of time-bin-entangled multiphoton states from a quantum emitter

Konstantin Tiurev ⬤,[*] Pol Llopart Mirambell ⬤, Mikkel Bloch Lauritzen ⬤, Martin Hayhurst Appel ⬤, Alexey Tiranov, Peter Lodahl, and Anders Søndberg Sørensen ⬤

Center for Hybrid Quantum Networks (Hy-Q), The Niels Bohr Institute, University of Copenhagen, DK-2100 Copenhagen Ø, Denmark

We analyze a scheme for generating multiphoton entangled states by a single solid-state quantum emitter and devise a mathematical framework for assessing the fidelity of the generated state. Within this formalism, we theoretically study the role of imperfections present in real systems on the generation of time-bin encoded Greenberger–Horne–Zeilinger and one-dimensional cluster states. We consider both fundamental limitations, such as the effect of phonon-induced dephasing, interaction with the nuclear spin bath, and second-order emissions, as well as technological imperfections, such as branching effects, nonperfect filtering, and photon losses. The devised framework is applicable to a range of quantum emitters, including semiconductor quantum dots, defect centers in solids, and atoms in cavities.

I. INTRODUCTION

A reliable source of entangled photons play a crucial role in future quantum technologies, ranging from photonic quantum computing [1–4] and communication [5–9] to fundamental tests of quantum mechanics [10–12]. Several approaches for the generation of such multiphoton entangled states exist. One particular method relies on the well-established technique for Bell state production via spontaneous parametric downconversion (SPDC) [13–15]. The Bell pairs can subsequently be joined into larger photonic states using quantum states fusion [16–18]. This approach is, however, inherently probabilistic and thus limited to entangling only a modest number of photons [19–22].

A highly promising direction for deterministic generation of large entangled states is to exploit a single quantum emitter efficiently coupled to light to directly produce entangled photons in a sequential manner [23–27]. In the proof-of-principle experiment by Schwartz *et al.* [28], it was inferred that entanglement between five subsequent polarization-encoded photons could be emitted by a single quantum dot. This founding experiment was conducted in a nonoptimized setting using metastable dark excitons as qubits and without implementing photonic nanostructures. Thus, the entangled states produced so far do not have sufficient quality to allow for all of the many envisioned applications. It is thus essential to understand the mechanisms affecting the quality of the produced states in order to determine how well this system can be scaled up for generating multiple high-fidelity qubits.

In this paper, we perform a detailed theoretical analysis of a protocol for the generation of the time-bin-entangled multiphoton states from a single quantum emitter. The specific scheme we consider was first implemented with quantum dots (QDs) in Ref. [27] albeit without being producing any

entanglement. It is particularly attractive for QDs because in contrast with previous proposals it can be implemented even with a strong magnetic field in the Voigt geometry. This improves the spin coherence properties of the spin states while simultaneously allowing optical rotations of the spin states. The same scheme has later been implemented with nitrogen vacancy centers in diamond [29]. The ideal protocol is described in Fig. 1. Such an ideal scenario is, however, always corrupted by imperfections that inevitably occur in real physical systems. In order to understand and minimize the imperfections present in actual implementations, we shall here investigate how these imperfections influence the generated states. We consider multiple sources of errors, which are shown in Fig. 2 and include (1) ground-state dephasing, (2) phonon-induced pure dephasing, (3) excitation errors, and (4) photon emission errors. We derive simple analytical expressions for evaluating the fidelity of the produced entangled states for a given physical system. This theoretical understanding of the imperfections can then be used to optimize experimental realizations both in terms of efficiency and quality of the produced states.

For concreteness we consider two types of multiphoton entangled states, Greenberger–Horne–Zeilinger (GHZ) and one-dimensional cluster states. The states will consist of N photons entangled with a single spin. For convenience we will label the state by the number of photons such that the N photon GHZ state will have the form

$$|\text{GHZ}^{(N)}\rangle = \frac{1}{\sqrt{2}}(|0\rangle^{\otimes N+1} + |1\rangle^{\otimes N+1}), \qquad (1)$$

which is a generalized version of Bell states to arbitrary number of particles. Here $|0\rangle$ and $|1\rangle$ denote logical states of the qubits. Being distributed over a network, this state allows for several interesting multiuser quantum protocols and thus serves a crucial resource for quantum network applications [30].

――――――
*konstantin.tiurev@gmail.com
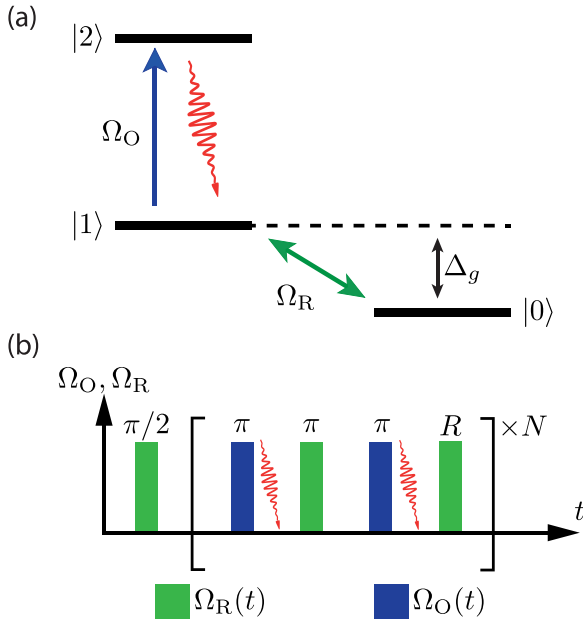
FIG. 1. Ideal protocol. (a) Idealized level structure and (b) driving pulse sequence for the generation of the GHZ states ($\hat{R} = \hat{X}$) or cluster states ($\hat{R} = \hat{H}$). Laser pulses Ω_O (green) and Ω_R (blue) are used for driving the optical transition $|1\rangle \leftrightarrow |2\rangle$ and for the ground-state rotations $|0\rangle \leftrightarrow |1\rangle$, respectively. Following each optical π-pulse, we wait for the excited state $|2\rangle$ to decay back to the ground state $|1\rangle$ (red wiggly lines). Using N repetitions of the pulse sequence, an entangled state of N photons and the quantum emitter is generated.

Cluster states have attracted a lot of attention as a universal resource for one-way quantum computation [1–4], and lately also as a promising resource for quantum repeaters [5,6,8]. In general cluster states can be obtained from arrays of qubits prepared in $|\Psi_0\rangle = (|0\rangle + |1\rangle)/\sqrt{2}$, by performing controlled phase gates between neighboring qubits along each of the dimensions of the cluster state. Unlike the GHZ state, cluster states do not allow for a compact-form expression since the number of terms grows rapidly with the number of qubits, but a two-qubit linear cluster state reads

$$|\text{Cluster}^{(1)}\rangle = \tfrac{1}{2}(|00\rangle + |01\rangle + |10\rangle - |11\rangle). \qquad (2)$$

This state can be transformed into $|\text{GHZ}^{(1)}\rangle$ using local unitary operation, but for $N > 1$ the state is in general much more complex. Most applications require two-dimensional cluster state, which in theory can be achieved by, e.g., making use of coupled emitters [31,32] or fusing multiple linear cluster states [33]. As a starting point, we focus in this work on the generation of linear cluster states, which can be achieved with a single emitter using the scheme in Fig. 1.

The reminder of this paper is organized as follows. In Sec. II we describe an idealized experimental protocol and introduce effective single-mode photon creation operators. In Sec. III we devise a theoretical formalism for calculation of the fidelities of the generated states. In Sec. IV we identify the main sources of imperfections expected to appear in real solid-state systems and derive expressions for corresponding
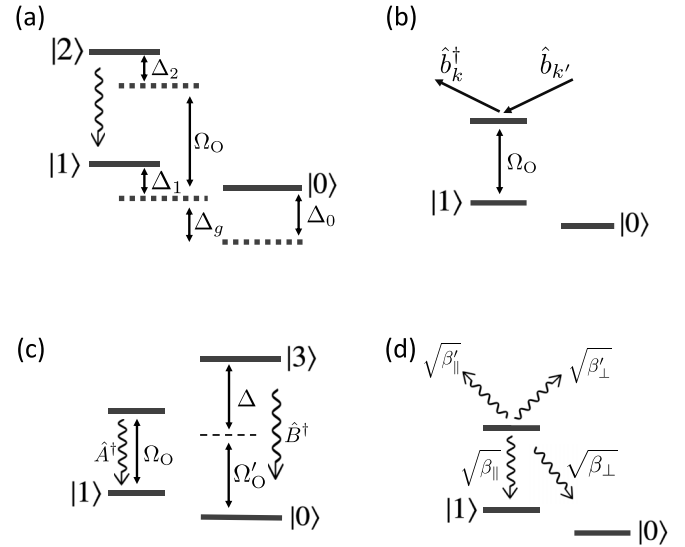
FIG. 2. Sources of imperfection. Errors considered include (a) level shifting induced by interaction with the nuclear spin bath, (b) phonon-induced pure dephasing, (c) second-order emissions from the resonant and far-detuned levels, and (d) branching errors due to alternative decay paths. See text for explanations of each of the effects.

infidelities. We assess the state fidelities for realistic experimental parameters and conclude with future perspectives in Sec. V.

II. IDEAL PROTOCOL

We begin with an idealized scheme proposed by Lee *et al.* [27] that uses a periodically driven quantum emitter for the sequential generation of photons entangled in their relative arrival times. The use of the time-bin degrees of freedom to encode and transfer quantum information is highly attractive since it is ideally suited for distribution through optical fibers. Furthermore, the scheme offers a number of advantages for quantum dots, but we expect that it will also be very suitable for other quantum emitters such as atoms in cavities [34–36] or color centers in diamond [29,37,38]. The scheme for the sequential generation of time-bin-entangled photons is illustrated in Fig. 1 and goes as follows:

(1) The ground-state spin is initialized in the state $|\Psi_0\rangle = (|0\rangle + |1\rangle)/\sqrt{2}$ using a $\pi/2$-pulse on the $|0\rangle \leftrightarrow |1\rangle$ transition using the field Ω_R.

(2) The $|1\rangle \leftrightarrow |2\rangle$ transition is resonantly driven by a π-pulse with the field Ω_O, which generates a photon in an early time bin $|e\rangle$ upon emission.

(3) The ground states $|0\rangle$ and $|1\rangle$ are flipped.

(4) Step 2 is repeated to generate a photon in a late time bin $|l\rangle$.

(5) GHZ state: step 3 is repeated.

Cluster state: the Hadamard gate (or, equivalently, a $\pi/2$ rotation around the x or y axis) between the ground states $|0\rangle$ and $|1\rangle$ is applied.

(6) Steps 2–5 are repeated N times to create an N-photon entangled state.

Following steps 2–5 for the GHZ state, the initial state transforms as

$$\frac{1}{\sqrt{2}}(|0,\emptyset\rangle + |1,\emptyset\rangle) \xrightarrow{2} \frac{1}{\sqrt{2}}(|0,\emptyset\rangle + |1,e\rangle)$$

$$\xrightarrow{3} \frac{1}{\sqrt{2}}(|1,\emptyset\rangle + |0,e\rangle) \xrightarrow{4} \frac{1}{\sqrt{2}}(|1,l\rangle + |0,e\rangle) \quad (3)$$

$$\xrightarrow{5} \frac{1}{\sqrt{2}}(|1,e\rangle + |0,l\rangle) = \frac{1}{\sqrt{2}}(\hat{A}_e^\dagger |1,\emptyset\rangle + \hat{A}_l^\dagger |0,\emptyset\rangle),$$

where $|\emptyset\rangle$ denotes the photon vacuum and the operator $\hat{A}_e^\dagger$ ($\hat{A}_l^\dagger$) creates a single photon in an early (late) time bin. Repeated N times, the protocol produces an $N+1$ particle GHZ state of the form (1) containing N photons and the spin. Here the spin state $|0\rangle$ ($|1\rangle$) and the photon state $|l\rangle$ ($|e\rangle$) are used as logical states $|0\rangle$ ($|1\rangle$). Replacing the π-pulse in the Step 5 with the Hadamard gate produces the state $(|0,l\rangle + |0,e\rangle + |1,e\rangle - |1,l\rangle)/2$, which is identical to Eq. (2). For higher N, the state is more complicated to write down, but we prove in Appendix A that the sequence produces a 1D-cluster state.

In the idealized protocol (3) described above, we do not go into details about the shape of the emitted photons. Taking a finite lifetime $1/\gamma$ of the excited state into account, the evolution during photon emission in the (u,j)th time interval can in a suitable rotating frame and under the Markov approximation be described by

$$|1,\emptyset\rangle \rightarrow \sqrt{\gamma} \int_0^\infty dt_e e^{-\frac{\gamma}{2} t_e} \hat{a}_{u,j}^\dagger(t_e) |1,\emptyset\rangle, \quad (4)$$

while the state $|0,\emptyset\rangle$ stays intact. Each time bin is labeled by indices (u,j), which correspond to the jth photon emitted in an early ($u = e$) or a late ($u = l$) part of the protocol. The operator $\hat{a}_{u,j}^\dagger(t_e)$ creates a photon at time t_e during the (u,j)th time interval. In principle the integral in Eq. (4) should not go to infinity since we will have a finite duration $T/2$ of the early and late time bin. We assume, however, that $\gamma T \gg 1$ so that we can ignore exponentially small terms $\exp(-\gamma t/2)$ for $t > T$ and extend the limit of the integration to infinity. Thus, the states after a single round of the protocol transform as in Eq. (3), with photon creation operators $\hat{A}_{u,j}^\dagger$ taking the form

$$\hat{A}_{u,j,\text{id}}^\dagger = \sqrt{\gamma} \int_0^\infty dt_e e^{-\frac{\gamma}{2} t_e} \hat{a}_{u,j}^\dagger(t_e), \quad (5)$$

which obey the correct bosonic operators commutation relations, $[\hat{A}_{u,j}, \hat{A}_{u',j'}^\dagger] = \delta_{u,u'}\delta_{j,j'}$.

For convenience, we define an ideal *single-round* operator

$$\hat{O}_{j,\text{id}}^\dagger = \hat{R}(|1\rangle\langle 0| \hat{A}_{l,j,\text{id}}^\dagger + |0\rangle\langle 1| \hat{A}_{e,j,\text{id}}^\dagger), \quad (6)$$

which corresponds to a single round of the protocol and, being applied to the spin state $|\Psi_0\rangle$, generates the jth photon in either the GHZ ($\hat{R} = \hat{X}$) or the cluster ($\hat{R} = \hat{H}$) state. The conventional notations $\hat{X}$ and $\hat{H}$ are used to denote the Pauli-X and Hadamard gates. The ideal N-photon states therefore read

$$\left|\Psi_{\text{id}}^{(N)}\right\rangle = \hat{O}_{N,\text{id}}^\dagger \cdots \hat{O}_{1,\text{id}}^\dagger |\Psi_0\rangle |\emptyset\rangle, \quad (7)$$

where $|\Psi_0\rangle$ is the initial spin state and $|\emptyset\rangle = |\emptyset_1 \cdots \emptyset_N\rangle$ is the N-photon vacuum.

In a realistic situation the generation process will introduce errors and imperfections. We will take this into account by modifying the single-round operator (6), which in the most

general case reads

$$\hat{O}_j^\dagger = |1\rangle\langle 0| \hat{A}_{10,e,j}^\dagger + |0\rangle\langle 1| \hat{A}_{01,e,j}^\dagger$$

$$+ |0\rangle\langle 0| \hat{A}_{00,e,j}^\dagger + |1\rangle\langle 1| \hat{A}_{11,e,j}^\dagger + (e \leftrightarrow l), \quad (8)$$

where the term in parentheses contains the same four terms with early replaced by late. Here $\hat{A}_{kl,j}^\dagger$ are general operators expressing the emission of photons for an emitter starting the jth period in state $|l\rangle$ and ending in state $|k\rangle$. The operators $\hat{A}_{kl,j}^\dagger$ contain all possible changes in the environment and the resulting leakage of information, e.g., due to phonon scattering or loss of photons during the pulse sequence. The environmental degrees of freedom are subsequently traced out when calculating the fidelity. This approach is slightly different than the typical master equation formalism, in which one traces over the environment from the beginning to achieve a reduced density matrix for the system. The difference between the two approaches is, however, only at which stage one traces over the environmental degrees of freedom and their results are equivalent.

In Sec. IV we take into account one imperfection at a time by constructing the corresponding operators (8) and calculate its effect on the quality of the produced state.

III. ENTANGLEMENT CHARACTERIZATION

A. Operational fidelity

Before moving to the sources of imperfections, we briefly describe the experimental measurement process and introduce the corresponding measure of how ideal the state is. The measure of closeness between two states is conventionally given by the fidelity, which is defined as

$$\mathcal{F}_{\text{exact}}^{(N)} = \text{Tr}_{\text{env}}\left\{\langle\Psi_{\text{id}}| \hat{\rho}^{(N)} |\Psi_{\text{id}}\rangle\right\}$$

$$= \text{Tr}_{\text{env}}\{\langle\Psi_{\text{id}}|\hat{O}_N^\dagger \cdots \hat{O}_1^\dagger |\Psi_0,\emptyset\rangle \langle\Psi_0,\emptyset| \hat{O}_1 \cdots \hat{O}_N |\Psi_{\text{id}}\rangle\},$$

$$(9)$$
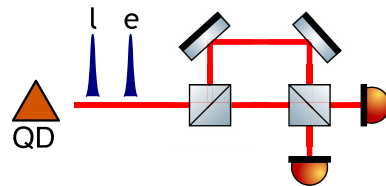
FIG. 3. Measurement setup for detecting time-bin-entangled photons. Measurements in the Z basis are made by passing both early and late photons through the short arm. For measurement in the X basis, the early and late photons are passed through the long and short arms of the interferometer, respectively. The measurement setup delays the early photon by a time equal to the time difference between the two excitation pulses, hence early and late photons arrive at the second beamsplitter at the same time when measured in the X (or Y) basis. The required photon routing can be done either passively by beamsplitters, or actively, e.g., using electro-optic modulators (EOMs). The former is experimentally simple but does not allow for a deterministic selection of the measurement basis as the wave packets are randomly reflected and transmitted at the first beamsplitter. The latter enables low loss measurement at repetition rates compatible with the typically achievable generation rates in our scheme.

where $|\Psi_{id}\rangle$ is the ideal state (7) produced by the operators in Eq. (6) and $\hat{\rho}^{(N)}$ is the output N-photon state produced by the operators (8). The trace over environment here corresponds to any unobserved degree of freedom, e.g., emitted phonons or lost photons.

Equation (9) compares the produced state with an outgoing photon in a well-defined temporal mode. In most experimental situations, however, one does not have complete information about the temporal mode. We will therefore slightly modify the strict definition of the fidelity (9) and introduce an *operational fidelity*. The typical experimental method of measuring time-bin-encoded qubits is to interfere a photon pulse with a time delayed pulse as shown in Fig. 3. In this interferometer, measurement in the Z-basis can be performed by letting both

the early and late photon wave packets pass through the short arm and recording the time of arrival. Alternatively the early time bin $|e\rangle$ can be routed to the long arm of the interferometer, while the late time bin $|l\rangle$ pass through the short arm. For a balanced interferometer the two wave packets thus arrive simultaneously at the last beamsplitter, enabling a measurement in the X or Y basis. Importantly, one distinguishes only between early and a late time bins, while the exact time of photon emission within each time bin is not resolved or discarded in the analysis. Thus, one effectively has two sets of indices labeling time: the number of the time bin j and the emission time within the time bin, t_j. Since the emission time is not used, we trace it out and obtain the *operational fidelity*,

$$\mathcal{F}^{(N)} = \mathrm{Tr}_{\mathrm{env}}\left\{ \int_0^\infty dt_N \cdots \int_0^\infty dt_1 \langle\emptyset| \langle\Psi_0| \hat{o}_1(t_1) \cdots \hat{o}_N(t_N) \hat{\rho}^{(N)} \hat{o}_N^\dagger(t_N) \cdots \hat{o}_1^\dagger(t_1) |\Psi_0\rangle |\emptyset\rangle \right\}$$

$$= \mathrm{Tr}_{\mathrm{env}}\left\{ \int_0^\infty dt_N \cdots \int_0^\infty dt_1 \langle\emptyset| \langle\Psi_0| \hat{o}_1(t_1) \cdots \hat{o}_N(t_N) \hat{O}_N^\dagger \cdots \hat{O}_1^\dagger |\Psi_0\rangle |\emptyset\rangle \langle\emptyset| \langle\Psi_0| \hat{O}_1 \cdots \hat{O}_N \hat{o}_N^\dagger(t_N) \cdots \hat{o}_1^\dagger(t_1) |\Psi_0\rangle |\emptyset\rangle \right\}, \quad (10)$$

where $\hat{\rho}^{(N)} = |\Psi^{(N)}\rangle \langle\Psi^{(N)}|$ is the real state defined in (9) and the operators

$$\hat{o}_j^\dagger(t_j) = \hat{R}(|1\rangle \langle 0| \hat{a}_{l,j}^\dagger(t_j) + |0\rangle \langle 1| \hat{a}_{e,j}^\dagger(t_j)) \quad (11)$$

are the projectors on the ideal GHZ ($\hat{R} = \hat{X}$) or cluster ($\hat{R} = \hat{H}$) states.

These two fidelity expressions (9) and (10) will in general give different results. Which of them provides a better description of concrete quantum information protocol will depend on the measurement performed in the specific protocol. If all photons are measured with a setup as in Fig. 3, then the fidelity in Eq. (10) provides a better description, whereas Eq. (9) may be a better choice if a different measurement sequence is used. As a specific example, the quantum repeater protocol of Ref. [8] considers photon numbers N in the range 200–300. Out of these only a single photon is interfered with a different quantum emitter, whereas the remaining $N - 1$ photons are measured in a setup as in Fig. 3. For this reason and since this is the experimentally most accessible quantity, we shall in the remainder of this article consider only the fidelity in Eq. (10).

B. Photon loss, filtering, and detection

The definition of the operational fidelity (10) is yet to be modified in order to correspond to an experimentally realistic measurements.

1. Photon losses

Successful detection of the emitted photons is limited by the collection of the photons from the waveguide, the subsequent propagation loss, and the detector efficiency. Due to these imperfections, experiments involving optical photons will have a nonzero probability to lose photons and only a fraction $\eta < 1$ of the produced photons will result in the detection event. We model loss of a photon by modifying the

single-mode creation operator (5) as

$$\hat{A}^\dagger \rightarrow \sqrt{\eta}\hat{A}^\dagger + \sqrt{1 - \eta}\hat{\tilde{A}}^\dagger, \quad (12)$$

where $\hat{\tilde{A}}^\dagger$ corresponds to the photons that do not reach the detector. In an experimental realization optical loss would lead to cases of unsuccessful entanglement generation and detection.

Photon loss is a major obstacle in most optical quantum information protocols. Therefore realistic schemes for quantum information processing involving single photons are designed to have built-in correction procedures against photon loss; see, e.g., Refs. [8,39]. By postselecting events where the correct number of photons are detected, unsuccessful photon detections are discarded in the quantum protocols and do not influence the fidelity of the successfully generated photons. We are therefore interested in computing the fidelity conditioned on the detection of a photon in each cycle. This corresponds to projecting the output state on the detected photon subspace, i.e., $\hat{O}_j^\dagger \rightarrow \hat{P}_{n_j>0} \hat{O}_j^\dagger$ with $\hat{P}_{n_j>0} = \hat{1} - |\emptyset\rangle \langle\emptyset|$. The probability of having a photon in each cycle of the protocol then reads

$$P(n_1 > 0, \ldots, n_N > 0) = \mathrm{Tr}\left\{\hat{P}_{n_1>0} \cdots \hat{P}_{n_N>0} \hat{\rho}^{(N)}\right\}. \quad (13)$$

Since we take into account only experimental realizations with nonzero measurements in each cycle of the protocol, the probability to accept an experimental realization will decrease, hence decreasing the probability of a successful outcome. The conditional fidelity is then given by normalising $\mathcal{F}^{(N)}$ to the total success probability (13),

$$\tilde{\mathcal{F}}^{(N)} = \frac{\mathcal{F}^{(N)}}{\mathrm{Tr}\left\{\hat{P}_{n_1>0} \cdots \hat{P}_{n_N>0} \hat{\rho}^{(N)}\right\}}. \quad (14)$$

The conditional fidelity above captures the quality of the state once the photons are successfully detected. The overall success probability does, however, influence the performance of any quantum protocol. For instance Ref. [8] describe a

quantum repeater protocol, which can in principle work for any single photon efficiency above 50% but assumes 95% for good performance, whereas the scheme for universal optical quantum computation in Ref. [39] tolerates a loss rate of 1.6%. These numbers are challenging to achieve, but solid-state implementations are beginning to reach this level with a recent experiment reaching 85% efficiency [40,41]. The efficiency is a separate issue from the quality and we here focus on the quality and evaluate the conditional fidelity. Alternatively the unconditional fidelity can be obtained from our results by simply multiplying the results with the associated success probability, which is essentially given by η^N.

2. Temporal filtering

In the ideal protocol (3) described above, the excitation $|1\rangle \rightarrow |2\rangle$ was considered to be instantaneous. Realistically, transferring population to the excited state takes the time of the Rabi π-cycle, which depends on the temporal shape and duration of the driving pulse. During this period photons from the driving laser can also leak into the detection arm of the setup. Thus, it is desirable to ignore the photons which were possibly emitted during the driving pulse or directly came from the laser. The undesired photons can be filtered out with near unit efficiency by keeping the detectors off during the driving laser pulse or by having shutters which admits photons only after the end of the excitation pulse.

3. Frequency filtering

The real systems have more complicated energy level structure than the scheme shown in Fig. 1(a). Not only the resonant transition is possible, but also emission of a photon from the far-detuned transitions, e.g., as in Fig. 2(c). In general, different transitions can have different collection efficiencies, which we take into account by redefining single-mode creation operators as

$$\hat{A}^\dagger \rightarrow \sqrt{\eta_2}\hat{A}^\dagger + \sqrt{1-\eta_2}\hat{\tilde{A}}^\dagger,$$
$$\hat{B}^\dagger \rightarrow \sqrt{\eta_3}\hat{B}^\dagger + \sqrt{1-\eta_3}\hat{\tilde{B}}^\dagger,$$

(15)

where $\eta_2 = \eta\xi_2$ and $\eta_3 = \eta\xi_3$ and the creation operators $\hat{A}^\dagger$ and $\hat{B}^\dagger$ correspond to the correct (resonant) and the undesired (off-resonant) photons, respectively. Without additional filtering, the photons from both transitions are collected with equal efficiency, i.e., $\xi_2 = \xi_3 = 1$. Cavity frequency filters can be added to the experimental setup in order to filter out the undesired photons and pass only the photons coming from the main transition. We will assume nonperfect filtering efficiency by applying filters such that $0 < \xi_3 \ll \xi_2 = 1$. Note that such (imperfect) frequency filtering is still compatible with perfect temporal filtering, e.g., if temporal shutters are placed before a frequency filter.

4. Detector dark counts

The fidelity at the detection stage can be affected by random detector dark counts. The effect of such dark counts depends on the efficiency $\eta_2\xi_2$ of collecting the desired photons. The effect is worst if the efficiency is low since in this limit the dark counts are competing with the relatively scarce photons counts. The dark counts effectively substitutes an (un-

detected) entangled photon with an uncorrelated photon with a probability $2NP_d$, where P_d is the dark count probability per pulse. Here the factor of $2N$ accounts for the early and late time bins of the N repetitions. This probability should be compared to probability of detecting a photon in the time window where the dark count happened. Since the random click has a probability $1/2$ of being in the right state this leads to a total infidelity $1 - \mathcal{F} = NP_d/(\eta_2\xi_2)$. Currently available detectors can have $P_d \approx 10^{-8}$ for pulses of duration of ≈ 2 ns. Hence even for relatively inefficient setups with $\eta_2\xi_2 \approx 1\%$ errors due to the detector dark counts are negligible compared to other effects we consider here.

A different type of dark counts appears due to background laser scattering into the detectors. These can be estimated by similar arguments to give $1 - \mathcal{F} = NP_b$, where P_b is the ratio of detected background photons to desired photons for a single excitation round. How this compares to imperfections from the intrinsic properties of the QD is heavily dependent on the experimental setup. We shall therefore not include it in the the discussion below.

In the reminder of this paper, we take into account different imperfections present in real systems by modifying the corresponding single-protocol operators (8) and calculating the fidelity according to Eqs. (10), (14), and (15).

IV. FIDELITY ASSESSMENT

A. Spin-state-preserving errors

We start our analysis by considering the errors that do not affect the spin states, but merely modify the single-mode creation operators (5) leaving the structure of the operators (6) unaffected. These include ground- and excited-state dephasing, two-photon emission, and excitation of the off-resonant transitions.

Inserting the GHZ-state operators (8) and (11) into (10) and assuming that the excitation at different time bins are uncorrelated, we obtain the unconditional fidelity of the GHZ state for non-spin-mixing errors,

$$\mathcal{F}^{(N)}[\text{GHZ}]$$
$$= \frac{1}{4}\text{Tr}_{\text{env}}\sum_{u,v=e,l}\left(\int_0^\infty dt\,\langle\emptyset|\,\hat{a}_u(t)\hat{A}_u^\dagger\,|\emptyset\rangle\,\langle\emptyset|\,\hat{A}_v\hat{a}_v^\dagger(t)\,|\emptyset\rangle\right)^N.$$

(16)

Analogously, the cluster state fidelity reads

$$\mathcal{F}^{(N)}[\text{Cl}]$$
$$= \text{Tr}_{\text{env}}\left(\frac{1}{4}\sum_{u,v=e,l}\int_0^\infty dt\,\langle\emptyset|\,\hat{a}_u(t)\hat{A}_u^\dagger\,|\emptyset\rangle\,\langle\emptyset|\,\hat{A}_v\hat{a}_v^\dagger(t)\,|\emptyset\rangle\right)^N.$$

(17)

The diagonal terms ($u = v$) in Eqs. (16) and (17) correspond to the z-basis measurement, while the off-diagonal terms ($u \neq v$) correspond to the x-basis measurement, as explained in Fig. 3. The expressions above are derived under an assumption that the creation operators $\hat{A}^\dagger$ at different time intervals commute. This assumption is valid as long as one considers coupling to a Markovian environment or a non-Markovian

classical noise, such as drift of the magnetic field or instability in the driving laser. The detailed derivations of the expressions (16) and (17) and a discussion of their applicability are given in Appendix B.

1. Ground-state dephasing

In solid-state emitters, both electron and hole spin states suffer from interaction with the nuclear spin bath, an effect also referred to as the Overhauser noise [42]. It results in a short spin coherence times T_2^*, which becomes a limiting factor for a number of quantum information processing applications. Effectively, the spin-bath induced noise adds a random shift Δ_i to the energy levels, as shown in Fig. 2(a). The corresponding perturbation of the three-level Hamiltonian is given by

$$\hat{H}' = \sum_{i=0}^{2} \Delta_i \, |i\rangle \, \langle i| . \tag{18}$$

Writing a wave-function ansatz as [43]

$$|\Psi(t)\rangle = c_2(t) |2, \emptyset\rangle + c_1(t) |1, \emptyset\rangle + c_0(t) |0, \emptyset\rangle$$
$$+ \int_0^\infty dt_e \phi(t, t_e) \hat{a}^\dagger(t_e) |0, \emptyset\rangle \tag{19}$$

and solving for coefficients $\phi(t, t_e), c_0(t)$ yields

$$\phi(t, t_e) = \sqrt{\gamma} e^{-i\Delta_1(t-t_e)} e^{-i\Delta_2 t_e} e^{-\frac{\gamma}{2} t_e} \theta(t - t_e)$$
$$c_0(t) = e^{-i\Delta_0 t} . \tag{20}$$

Thus, the states after the first half of the protocol transform according to

$$|1, \emptyset\rangle \rightarrow \sqrt{\gamma} e^{-i\frac{\Delta_1 T}{2}} \int_0^\infty dt_e e^{-\frac{\gamma}{2} t_e} e^{-i\Delta_{21} t_e} \hat{a}_{u,j}^\dagger(t_e) |1, \emptyset\rangle ,$$

$$|0, \emptyset\rangle \rightarrow e^{-i\frac{\Delta_0 T}{2}} |0, \emptyset\rangle , \tag{21}$$

where we denote $\Delta_{21} = \Delta_2 - \Delta_1$. Note that after a single full round of the protocol, both $|0\rangle$ and $|1\rangle$ states will accumulate a global phase $e^{-i(\Delta_0 + \Delta_1)T/2}$, which is not important and can be omitted. The initial state $|\Psi_0\rangle$ therefore transforms according to the ideal protocol (3), where the single-mode operators $\hat{A}_{u,j}^\dagger$ are defined as

$$\hat{A}_{u,j}^\dagger = \sqrt{\gamma} \int_0^\infty dt \, e^{-\frac{\gamma}{2} t} e^{-i\Delta_{21} t} \hat{a}_{u,j}^\dagger(t) . \tag{22}$$

With these operators, each of the four terms in Eqs. (16) and (17) yields

$$\int_0^\infty dt \, \langle \emptyset | \hat{a}_u(t) \hat{A}_u^\dagger |\emptyset\rangle \, \langle \emptyset | \hat{A}_v \hat{a}_v^\dagger(t) |\emptyset\rangle$$
$$= \gamma \int_0^\infty dt \int_0^\infty dt' \int_0^\infty dt'' \underbrace{\langle \emptyset | \hat{a}_u(t) \hat{a}_u^\dagger(t') |\emptyset\rangle}_{\delta(t-t')}$$
$$\underbrace{\langle \emptyset | \hat{a}_v(t'') \hat{a}_v^\dagger(t) |\emptyset\rangle}_{\delta(t-t'')} e^{-\frac{\gamma}{2}(t'+t'')} e^{i\Delta_{12}(t'-t'')} = 1, \tag{23}$$

and therefore

$$\mathcal{F}_{T_2^*}^{(N)}[\text{GHZ}] = \mathcal{F}_{T_2^*}^{(N)}[\text{Cl}] = 1. \tag{24}$$

Strikingly, dephasing induced by the interaction with the nuclear spin bath or any other slow drift of the energy levels does not affect the quality of the produced state. This happens due to two reasons. First, as was pointed out earlier, the duration of the early and late parts of the protocol are equal, resulting in common global phase $e^{-i(\Delta_0 + \Delta_1)T/2}$, which we omit. This is reminiscent to a spin echo built into the time-bin generation protocol [44–46]. Second, the experiment does not resolve the exact photon emission time, but only the number of a time bin, i.e., the change from the fidelity definition in Eq. (9) to the fidelity in Eq. (10). Here we interfere only photons which are emitted exactly $T/2$ apart using the interferometer in Fig. 3. This means that the interfered photons come from events which have spent exactly the same time in the excited states, ensuring perfect spin echo conditions. Alternatively this effect can also be understood from the indistinguishability of the photons: The ground-state dephasing results from drifts in the energy levels. These drifts lead to a spread in the frequency of the photons. Two photons emitted shortly after each other will however have the same frequency since the energy levels are assumed not to drift on this small time scale. The two photon wave packets interfered by the interferometer in Fig. 3 are thus perfectly indistinguishable, resulting in no reduction in the interference. We note, however, that this effect is linked to this particular experimental configuration. If we are, e.g., interfering photons emitted from different emitters, this effect may not be applicable and the more strict fidelity defined in Eq. (9) may provide a more appropriate characterization.

The immediate consequence of Eq. (24) in the context of quantum dot emitters is that while the coherence time of a hole spin is considerably longer than that of an electron, the dephasing is effectively removed in the protocol and both the electron spin and the hole spin can be used as the ground-state qubit with equally good performance.

Above we used the fact that the drift of the energy levels due to the Overhauser effect happens on the timescales much slower than a single round of the protocol and thus can be neglected. On longer times, however, such drift can potentially influence the coherence and is often referred to as T_2 noise. However, in our protocol the π-pulses are periodically applied in the middle of each repetition of the protocol, which has been shown to increase T_2 to few microseconds, thus suppressing the corresponding noise [47,48] even if the number of produced photons is scaled to hundreds for typical quantum dot emission timescales. We thus expect slow drifts of energy levels to have a negligible effect on the quality of the produced multiphoton states and do not consider this type of dephasing.

2. Phonon-induced pure dephasing

The next imperfection we study is pure dephasing of the excited state induced by scattering of phonons, as shown in Fig. 2(b). While the spin is excited, it can scatter phonons thereby inducing a random phase change at a rate γ_d. This phonon scattering can take place both during the excitation pulse and in the period after the excitation, where the emitter is undergoing spontaneous emission. Since the duration of the excitation pulse needs to be much shorter than the lifetime of the excited state, the effects of dephasing during excitation

pulse will be ignored. The wave function corresponding to a single emitted photon and one scattered phonon can be described as

$$|\Psi\rangle_{u,j} = \int_0^\infty dt_e \left(\phi(t_e) + \sum_k \phi_k(t_e) \hat{b}_{u,j,k}^\dagger \right) \hat{a}_{u,j}^\dagger(t_e) |1, \emptyset, \tilde{\emptyset}\rangle ,$$

(25)

where $|\tilde{\emptyset}\rangle$ denotes the vacuum state of phonons, $u = \{e, l\}$, and j is the photon number. The operator $\hat{b}_{u,j,k}^\dagger$ creates a phonon in mode k and $\langle\tilde{\emptyset}| \hat{b}_{u,j,k} \hat{b}_{u',j',k'}^\dagger |\tilde{\emptyset}\rangle = \delta_{u,u'}\delta_{j,j'}\delta_{k,k'}$, i.e., we make a Markovian approximation for the phononic reservoir such that phonons scattered in different time bins or different modes are orthogonal. In Eq. (25) we model only a first-order scattering process and neglect the probabilities to scatter more than one phonon per cycle. Since the scattering of even a single phonon will remove all coherence with the excited states, the scattering of a second phonon will not further reduce the fidelity and it is sufficient to consider the scattering of a single. The coefficients in Eq. (25) were derived in Ref. [49] and read

$$\phi(t_e) = \sqrt{\gamma} e^{-(\frac{\gamma}{2}+\gamma_d)t_e}$$

$$\sum_k |\phi_k(t_e)|^2 = \gamma e^{-\gamma t_e}(1 - e^{-2\gamma_d t_e}).$$

(26)

As in the case of ground-state dephasing, phonon scattering does not alter the spin states and merely modifies the single-mode operators (5) which now read

$$\hat{A}_{u,j}^\dagger = \int_0^\infty dt_e \left(\phi(t_e) + \sum_k \phi_k(t_e) e^{-i\omega_k t_e} \hat{b}_{u,j,k}^\dagger \right) \hat{a}_{u,j}^\dagger(t_e).$$

(27)

Substituting single-mode operators (27) and the coefficients (26) into the off-diagonal terms of Eqs. (16) and (17) yields

$$\mathrm{Tr}_{\mathrm{ph}}\left\{ \int_0^\infty dt \, \langle\emptyset| \hat{a}_u(t) \hat{A}_u^\dagger |\emptyset, \tilde{\emptyset}\rangle \langle\emptyset, \tilde{\emptyset}| \hat{A}_v \hat{a}_v^\dagger(t) |\emptyset\rangle \right\}$$

$$= \int_0^\infty dt |\phi(t)|^2 = \frac{\gamma}{\gamma + 2\gamma_d},$$

(28)

where $u \neq v$. In Eq. (28) only the terms that do not contain the phonon creation operators $\hat{b}^\dagger$ survive since phonons scattered in an early and a late time bins are orthogonal. The diagonal terms of Eqs. (16) and (17) with the coefficients (26) become unity,

$$\mathrm{Tr}_{\mathrm{ph}}\left\{ \int_0^\infty dt \, \langle\emptyset| \hat{a}_u(t) \hat{A}_u^\dagger |\emptyset, \tilde{\emptyset}\rangle \langle\emptyset, \tilde{\emptyset}| \hat{A}_u \hat{a}_u^\dagger(t) |\emptyset\rangle \right\}$$

$$= \int_0^\infty dt \left(|\phi(t)|^2 + \sum_k |\phi_k(t)|^2 \right) = 1,$$

(29)

where no cross terms of the form $\phi(t)\phi_k^*(t)$ are present since $\mathrm{Tr}_{\mathrm{ph}}\{\hat{b}_{u,j,k}^\dagger |\tilde{\emptyset}\rangle \langle\tilde{\emptyset}|\} = 0$.

Finally, inserting (28) and (29) into Eqs. (16) and (17) yields the fidelity of the N-photon GHZ and cluster states in
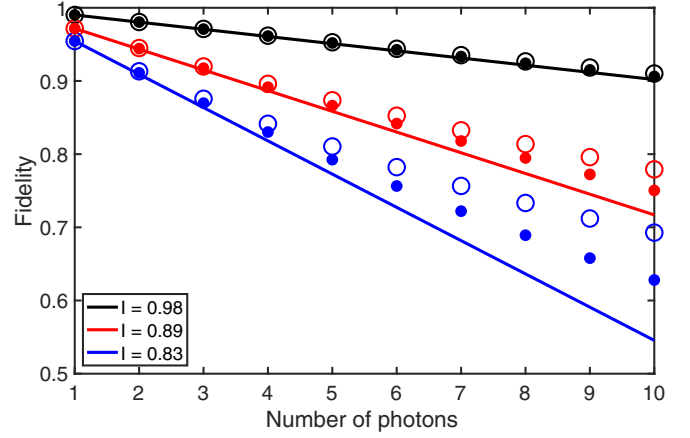
FIG. 4. Fidelities of the GHZ (circles) and the cluster (dots) states in the presence of phonon dephasing. The first-order approximation (31) for both the GHZ and the cluster state is shown with solid lines and agrees well with the exact solution (30) for a large fidelity $\mathcal{F} \gtrsim 0.8$. Black, red, and blue curves correspond to the dephasing rates $\gamma_d/\gamma = 0.01$, $\gamma_d/\gamma = 0.03$, and $\gamma_d/\gamma = 0.05$, respectively.

the presence phonon-induced pure dephasing,

$$\mathcal{F}_{\mathrm{ph}}^{(N)}[\mathrm{GHZ}] = \frac{1}{2} + \frac{1}{2}\left(\frac{\gamma}{\gamma + 2\gamma_d} \right)^N = \frac{1 + I^N}{2},$$

$$\mathcal{F}_{\mathrm{ph}}^{(N)}[\mathrm{Cl}] = \frac{1}{2^N}\left(1 + \frac{\gamma}{\gamma + 2\gamma_d} \right)^N = \left(\frac{1 + I}{2} \right)^N, \quad (30)$$

where the degree of indistinguishability is defined as $I = \gamma/(\gamma + 2\gamma_d)$ [50]. Since typically $\gamma_d \ll \gamma$, the expressions above can be expanded around $\gamma_d/(\gamma + 2\gamma_d) = 0$. In the first-order approximation, the fidelities of the two states become identical,

$$\mathcal{F}_{\mathrm{ph,approx}}^{(N)} = 1 - N\frac{\gamma_d}{\gamma + 2\gamma_d} = 1 - N\frac{1 - I}{2}. \quad (31)$$

Figure 4 shows plots of the fidelities for a realistic range of parameters and different number of photons.

3. Excitation errors

Next, we take into consideration the errors that can occur during the excitation of the transition $|1\rangle \leftrightarrow |2\rangle$. The possible errors consist of two components. First is the probability of emitting a photon already during the finite duration of the driving laser pulse used to excite the $|1\rangle \leftrightarrow |2\rangle$ transition. In the discussion above, the excitation process was considered to be instantaneous and photons were retrieved only during the relaxation time of the protocol following the pump pulse. However, photon emissions during the driving pulse are possible and should be taken into account. We assume temporal filtering by keeping detectors inactive while driving the system to the excited state, as discussed in Sec. III B. Hence photons emitted during the driving pulses are assumed to be lost and we consider only photons emitted during the subsequent period of free decay.

A second source of imperfection considered here is the probability of exciting a far-detuned transition $|0\rangle \leftrightarrow |3\rangle$ as shown in Fig. 2(c). Cavity filters are assumed to suppress

contributions from off-resonant photons emitted on this transition, but the excitation of this will still induce dephasing due to multiphoton emission and the filtering may not be perfect. Hence we need to evaluate the effect of this.

We note that the two effects depend on the temporal shape and length of the driving laser pulse in opposite ways: short high-intensity pulses would allow to highly suppress the second-order photon emission at the cost of strongly driving the undesired $|0\rangle \leftrightarrow |3\rangle$ transition. On the

other hand, long and weak driving pulses can suppress the excitation of the off-resonant transition but will result in photon emission during the pulse. Thus, our goal here is twofold: (1) to find an optimal regime of the driving laser and (2) to evaluate the corresponding fidelity of multiphoton states.

An extensive analysis of this system is provided in Ref. [51]. Below we merely outline the central results. We start by writing a wave-function ansatz as [43]

$$|\Psi_{eg}\rangle = c_g(t)\,|g, \varnothing\rangle + c_e(t)\,|e, \varnothing\rangle + \int dt_e \phi_g(t, t_e)\hat{a}^\dagger[v_g(t - t_e)]\,|g, \varnothing\rangle + \int dt_e \phi_e(t, t_e)\hat{a}^\dagger[v_g(t - t_e)]\,|e, \varnothing\rangle$$

$$+ \int dt_{e_1} \int dt_{e_2} \phi_{gg}(t, t_{e_1}, t_{e_2})\hat{a}^\dagger[v_g(t - t_{e_1})]\hat{a}^\dagger[v_g(t - t_{e_2})]\,|g, \varnothing\rangle, \tag{32}$$

where $\hat{a}^\dagger(z) = \frac{1}{\sqrt{2\pi}} \int dk \hat{a}_k^\dagger e^{i(k-k_0)z}$ is the creation operator in real space and v_g is the group velocity. The first three terms in Eq. (32) are analogous to the scenario described by Eq. (19) and include excited- and ground-states amplitudes $c_g(t)$ and $c_e(t)$ and the first-order photon emission process [ϕ_g]. The wave function (32) furthermore considers the possibility to emit a photon during the pulse and to be re-excited [ϕ_e], and the possibility to emit one photon during and one photon after the pulse [ϕ_{gg}]. Since we currently do not consider the possibility of transitions between the two branches $|1\rangle \leftrightarrow |2\rangle$ and $|0\rangle \leftrightarrow |3\rangle$, the wave-function ansatz (32) can be written and solved separately for the resonant two-level system ($\{g, e\} = \{1, 2\}$) and the undesired far-detuned transition ($\{g, e\} = \{0, 3\}$).

Taking into account all possible outcomes, the states upon photon emission become

$$|1, \varnothing\rangle \rightarrow \left(c_1 + c_2\hat{A}_0^\dagger + \Phi_1\hat{A}_{p_1}^\dagger + \Phi_2\hat{A}_{p_2}^\dagger\hat{A}_0^\dagger\right)|1, \varnothing\rangle,$$

$$|0, \varnothing\rangle \rightarrow \left(c_0 + c_3\hat{B}_0^\dagger + \Phi_0\hat{B}_{p_1}^\dagger + \Phi_3\hat{B}_{p_2}^\dagger\hat{B}_0^\dagger\right)|0, \varnothing\rangle, \tag{33}$$

where the coefficients Φ_i are such that $|\Phi_i(T_p)|^2 = v_g \int dt_e |\phi_i(T_p, t_e)|^2$. The creation operators $\hat{A}^\dagger$ ($\hat{B}^\dagger$) correspond to emission of a photon from the resonant $|1\rangle \leftrightarrow |2\rangle$ (off-resonant $|0\rangle \leftrightarrow |3\rangle$) transition during ($\hat{A}_{p_i}^\dagger$, $\hat{B}_{p_i}^\dagger$) or after ($\hat{A}_0^\dagger$, $\hat{B}_0^\dagger$) the pulse. For simplicity we have here ignored the possibility of two photons being emitted during the pulse. We therefore evaluate the wave function in Eq. (32) at the end of the pulse at time T_p keeping at most a single emission during the pulse. After this time the system will emit a photon if it is in the excited states. This emission process is independent of the dynamics during the excitation process and is the denoted by the same operators A_0 and B_0 irrespective of the dynamics during the pulse. Furthermore all coefficients are to be evaluated at the end of the pulse T_p. A single round of the protocol therefore corresponds to the action of an operator

$$\hat{O}_j^\dagger = \hat{R}(|1\rangle\langle 0|\,\hat{Q}_{l,j}^\dagger + |0\rangle\langle 1|\,\hat{Q}_{e,j}^\dagger), \tag{34}$$

which has the same form as (8) with the single-mode operators $\hat{A}_{u,j}^\dagger$ replaced by the effective creation

operators

$$\hat{Q}_{u,j}^\dagger = \left(c_1 + c_2\hat{A}_0^{\dagger,u} + \Phi_1\hat{A}_{p_1}^{\dagger,u} + \Phi_2\hat{A}_{p_2}^{\dagger,u}\hat{A}_0^{\dagger,u}\right)_j$$

$$\times \left(c_0 + c_3\hat{B}_0^{\dagger,v} + \Phi_0\hat{B}_{p_1}^{\dagger,v} + \Phi_3\hat{B}_{p_2}^{\dagger,v}\hat{B}_0^{\dagger,v}\right)_j, \tag{35}$$

where j is a photon number and $\{u, v\} = \{e, l\}$, $u \neq v$.

The operator (35) includes all possible combinations of photons emitted from two two-level systems in a single round of the protocol. An ideal noiseless protocol corresponds to a single photon coming from the resonant transition, i.e., to $\hat{Q}_{u,\text{ideal}}^\dagger = \hat{c}_2\hat{c}_0\hat{A}_0^{\dagger,u}$ with $|c_0| = |c_2| = 1$. In order to improve the quality of the produced state, we consider a combination of temporal and spectral filters to the output state (34), which suppress contributions from the terms other than $\hat{c}_2\hat{c}_0\hat{A}_0^{\dagger,u}$ in (35) as discussed in Sec. III B. First, we accept only experimental instances which contain at least one photon emitted after the driving pulse, i.e., we reject states that do not contain $\hat{A}_0^\dagger$ or $\hat{B}_0^\dagger$ in (34) at each round of the protocol. Next, we use frequency filters to reject the photons emitted at the correct time but with off-resonant frequency, that is, we suppress the contribution from the $\hat{B}_0^\dagger$ as described in Eq. (15).

The full state after applying the temporal and frequency filters to the state is given in Appendix C. The single-protocol operators (35) do not mix the spin states, and therefore the expressions for the fidelities (16) and (17) are still valid, with photons emitted during the pulse playing the role of an environment. Since photons from different time bins are orthogonal, the only term that survives the trace operation in the off-diagonal terms of Eqs. (16) and (17) is

$$D_1 = \text{Tr}_p\left\{ \int_0^\infty dt \,\langle\varnothing|\,\hat{a}_v(t)\hat{Q}_{v,j}^\dagger\,|\varnothing\rangle\,\langle\varnothing|\,\hat{Q}_{u,j}\hat{a}_u^\dagger(t)\,|\varnothing\rangle \right\}$$

$$= \eta_2|c_0c_2|^2 \tag{36}$$

with $u \neq v$. The diagonal terms read

$$D_2 = \text{Tr}_p\left\{ \int_0^\infty dt \,\langle\varnothing|\,\hat{a}_u(t)\hat{Q}_{u,j}^\dagger\,|\varnothing\rangle\,\langle\varnothing|\,\hat{Q}_{u,j}\hat{a}_u^\dagger(t)\,|\varnothing\rangle \right\}$$

$$= \eta_2(|c_0c_2|^2 + |c_0\Phi_2|^2 + |\Phi_0c_2|^2 + |\Phi_0\Phi_2|^2)$$

$$+ \eta_2(1 - \eta_3)(|c_2c_3|^2 + |\Phi_2c_3|^2 + |\Phi_3c_2|^2 + |\Phi_3\Phi_2|^2). \tag{37}$$
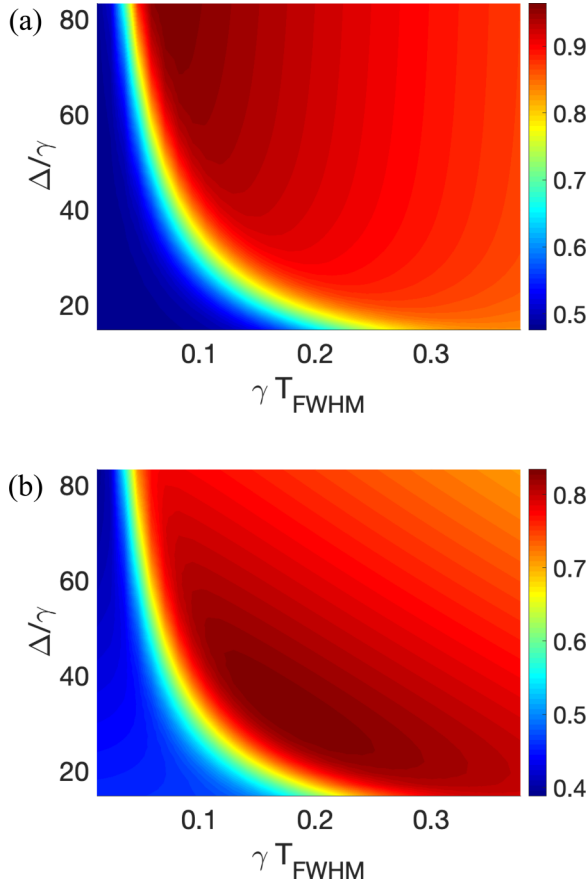
FIG. 5. Conditional fidelities of the five-photon GHZ state for a Gaussian-shaped pulse as a function of the pulse length γT_{FWHM} (x axis) and lifetime of the excited state, Δ/γ (y axis) at a fixed $\Delta = 2\pi \times 16$ ns^{-1}. Panels (a) and (b) correspond to the fidelity with excitation errors $\tilde{\mathcal{F}}_{\mathrm{exc}}$ only and to the combined fidelity $\tilde{\mathcal{F}}_{\mathrm{comb}}$, respectively. In (b) we have assumed a ratio of $\Delta/\gamma_d = 1.7 \times 10^3$, which roughly corresponds to quantum dots in a 2 T magnetic field at a temperature of 1.8 K.

Finally, postselection is taken into account by dividing the fidelity by the success probability, i.e., the probability that at least one photon has been detected,

$$P(n_j > 0) = D_2 + D_3, \tag{38}$$

where

$$\begin{aligned} D_3 = \eta_3 (&|c_3 c_1|^2 + |c_3 \Phi_1|^2 + |\Phi_3 c_1|^2 + |\Phi_3 \Phi_1|^2 \\ &+ |c_3 c_2|^2 + |c_3 \Phi_2|^2 + |\Phi_3 c_2|^2 + |\Phi_3 \Phi_2|^2). \end{aligned} \tag{39}$$

Substituting Eqs. (36)–(39) into (14) yields the conditional fidelities of the GHZ and the cluster states,

$$\tilde{\mathcal{F}}_{\mathrm{exc}}^{(N)}[\mathrm{GHZ}] = \frac{1}{2} \frac{D_1^N + D_2^N}{(D_2 + D_3)^N},$$

$$\tilde{\mathcal{F}}_{\mathrm{exc}}^{(N)}[\mathrm{Cl}] = \frac{1}{2^N} \left(\frac{D_1 + D_2}{D_2 + D_3} \right)^N. \tag{40}$$

The detailed derivations of Eqs. (36)–(39) are provided in Appendix C.

The final step is the calculation of the coefficients in Eq. (40), which depend on the temporal shape of the driv-

ing light pulse, photon emission rate γ, detuning Δ, and filtering efficiencies ξ_2, ξ_3. In the Appendix C, we provide a system of coupled differential equations for the coefficients $\{c_i(t), \Phi_i(t)\}$, which where solved numerically under the assumption that the driving laser pulse has a Gaussian temporal profile. Figure 5(a) shows the calculated conditional fidelity of the five-photon GHZ state. We vary the emission rate γ and full width half maximum pulse length T_{FWHM} while keeping a fixed detuning of the state $|3\rangle$ from the resonant transition. To ensure that we have a finite pulse duration, experiments will have to truncate the Gaussian pulse. In our simulation we do this at $T_{\mathrm{p}} = 3.2 \times T_{\mathrm{FWHM}}$. Choosing a too long pulse duration will affect the success probability since the excitation in the excited state will decay, and hence a compromise will have to be made between the truncation of the Gaussian and the success probability.

As follows from Fig. 5(a), reducing the emission rate γ at fixed values of the detuning Δ and γT_{FWHM} improves the fidelity of the state. On the other hand, according to Eq. (30), increasing the emission rate results in a higher dephasing fidelity since the system spends less time in the excited state. Therefore, we show the combined fidelity $\tilde{\mathcal{F}}_{\mathrm{comb}} = \mathcal{F}_{\mathrm{ph}} \tilde{\mathcal{F}}_{\mathrm{exc}}$ in Fig. 5(b) assuming fixed values $\Delta = 2\pi \times 16$ ns^{-1} and $\gamma_d = 0.06$ ns^{-1}. The calculated optimal parameters are $T_{\mathrm{FWHM,opt}} = 0.06$ ns and $\gamma_{\mathrm{opt}} = 3.2$ ns^{-1}, which corresponds to a degree of indistinguishability $I_{\mathrm{opt}} = 0.96$ and falls within the experimentally realistic range of parameters for quantum dots. Figure 5 shows only the results for the GHZ state since the fidelity of the cluster state is almost identical in the considered range of parameters. Figure 6(a) shows comparison between the fidelities with and without frequency filters. Evidently, frequency filters have a very small effect on the excitation errors in the assumed range of experimental parameters, but as shown below it will have a much larger effect on the branching error.

In Appendix C we also derive an analytical solution corresponding to the simplified model where (1) a square-shaped driving pulse is used, (2) frequency filters have perfect efficiency, $\xi_2 = 1, \xi_3 = 0$, and (3) dynamics is solved up to the first order in perturbation theory. Furthermore we chose the pulse duration and intensity such that a perfect π-pulse is achieved on the resonant transition, whereas the off-resonant transition perform an off-resonant 2π Rabi oscillation, ideally returning all amplitude from state $|3\rangle$ to state $|0\rangle$. With these assumptions, the conditional fidelity reads

$$\tilde{\mathcal{F}}_{\mathrm{exc,sq}}^{(N)} = 1 - N \frac{\sqrt{3}\pi}{8} \frac{\gamma}{\Delta}. \tag{41}$$

Using a square shape approximation of the driving laser pulse serves as a good approximation and gives a simple analytical expression for the fidelity at optimal parameters, as one can observe in Fig. 6(b).

B. Branching error

In the preceding discussion, we have assumed that only the vertical transitions in Fig. 2(c) were allowed. This section is devoted to studying a more complex decay structure.

First, we study how imperfect decay ratios affect the quality of the generated quantum state. A level diagram with an
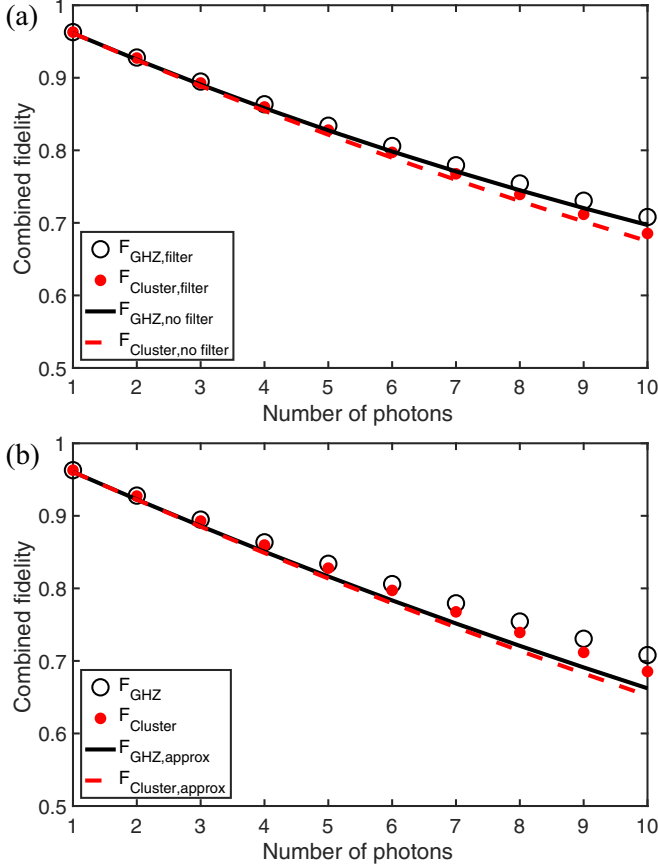
FIG. 6. (a) Effect of frequency filtering. Optimized combined fidelities of the GHZ (circles) and the cluster (dots) states as a function of a number of photons with frequency filters such that $\eta_2 = 1$, $\eta_3 = 0.02$. Solid and dashed lines correspond to, respectively, the GHZ and the cluster state without frequency filtering. (b) Validity of the first-order and square-shaped pulse approximations. Comparison between the combined fidelity of the GHZ state from the exact numerical solution for a Gaussian driving pulse (40) (circles) and its first-order approximation for a square pulse (41) (black solid line), respectively. The exact and first-order fidelities of the cluster state are shown with red dots and dashed lines, respectively. Parameters values are given in the text.

additional decay path is shown in Fig. 2(d). Since the excitation of the level $|3\rangle$ in Fig. 2(c) constitute an error in itself, we will ignore a similar additional decay path from this level and focus on the level scheme in Fig. 2(d). We characterize the two decay paths by parameters $\beta_\parallel$ and $\beta_\perp$, which are the probabilities to emit a photon into the waveguide through the correct ($|2\rangle \rightarrow |1\rangle$) or the incorrect diagonal ($|2\rangle \rightarrow |0\rangle$) transition, respectively.

Next, we consider photon losses, which we will divide into intrinsic and extrinsic losses. Intrinsic losses correspond to the photon emitted through the vertical or the diagonal transition out of the waveguide mode, corresponding to two additional processes shown in Fig. 2(d). The two processes occur with probabilities $\beta'_\parallel$ and $\beta'_\perp$ for the desired and undesired transition, respectively. Extrinsic losses were discussed in Sec. III B and correspond to the overall efficiency η of the experimental setup and include all possible losses between the waveguide

and the detector. Taken together, the probabilities to emit and detect a photon coming from either the vertical or the diagonal transition are given by

$$p_\parallel = \eta_2 \beta_\parallel, \qquad p_\perp = \eta_3 \beta_\perp, \tag{42}$$

while the probabilities of losing the corresponding photons are

$$p'_\parallel = \beta'_\parallel + (1 - \eta_2)\beta_\parallel,$$
$$p'_\perp = \beta'_\perp + (1 - \eta_3)\beta_\perp, \tag{43}$$

where $\eta_i = \eta \xi_i$, $\eta \leqslant 1$, and $\xi_i = 1$ ($\xi_i \ll 1$) without (with) frequency filters on the ith transition. The full state after a single round of the protocol then reads

$$|\Psi^{(1)}\rangle = \frac{1}{\sqrt{2}} \hat{R} \big(|0\rangle \{ \sqrt{p_\parallel}\, |e, \varnothing\rangle + \sqrt{p'_\parallel}\, |1_{e\parallel}, \varnothing\rangle + \sqrt{p_\perp}\, |l', \varnothing\rangle$$

$$+ p_\perp |l', e'\rangle + \sqrt{p_\perp p'_\perp}\, |l', 1_{e\perp}\rangle$$

$$+ \sqrt{p'_\perp}\, |1_{l\perp}, \varnothing\rangle + \sqrt{p_\perp p'_\perp}\, |e', 1_{l\perp}\rangle + p'_\perp |1_{e\perp}, 1_{l\perp}\rangle \}$$

$$+ |1\rangle \{ \sqrt{p_\parallel}\, |l, \varnothing\rangle + \sqrt{p_\parallel p_\perp}\, |l, e'\rangle + \sqrt{p_\parallel p'_\perp}\, |l, 1_{e\perp}\rangle$$

$$+ \sqrt{p'_\parallel}\, |1_{l\parallel}, \varnothing\rangle + \sqrt{p'_\parallel p_\perp}\, |e', 1_{l\parallel}\rangle$$

$$+ \sqrt{p'_\parallel, p'_\perp}\, |1_{l\parallel}, 1_{e\perp}\rangle \} \big), \tag{44}$$

where $|e'\rangle$ and $|l'\rangle$ are, respectively, early and late photons emitted into the waveguide through the diagonal $|2\rangle \rightarrow |0\rangle$ transition of Fig. 2(d) and $|1_{u\parallel}\rangle$ ($|1_{u\perp}\rangle$) denotes a late ($u = l$) or an early ($u = e$) photon that has been lost after being emitted in a vertical (diagonal) transition. Again the operator $\hat{R}$ is $\hat{X}$ and $\hat{H}$ for the GHZ and the cluster state, respectively. As expected, Eq. (44) reduces to the ideal state (7) for $p_\parallel = 1$ and $p_\perp = p'_\perp = p'_\parallel = 0$.

The expressions for the fidelities (16) and (17) were derived under the assumptions that only the vertical transitions between spin states were allowed, and are thus not valid when imperfect branching in Fig. 2(d) is taken into account. We thus need to derive new expressions for the fidelity in this case. This calculation is different for the GHZ and cluster states, and will thus be handled separately below.

1. GHZ state with branching errors

We start by calculating the fidelity of the GHZ state, which corresponds to $\hat{R} = \hat{X}$ in Eqs. (44) and (11). Using the same formalism as in the previous sections, the single round operators that produce a correct GHZ state read

$$\hat{O}_j^\dagger = |1\rangle\langle 1| \big(\sqrt{p_\parallel} \hat{A}_{e,j}^\dagger + \sqrt{p'_\perp p_\perp} \hat{A}_{e',j}^\dagger \hat{L}_j^\dagger \big)$$

$$+ |0\rangle\langle 0| \sqrt{p_\parallel} \hat{A}_{l,j}^\dagger + |0\rangle\langle 1| \sqrt{p'_\perp p_\parallel} \hat{A}_{l,j}^\dagger \hat{E}_j^\dagger, \tag{45}$$

where $\hat{L}_j^\dagger = |1_{l\perp,j}\rangle\langle\varnothing|$ and $\hat{E}_j^\dagger = |1_{e\perp,j}\rangle\langle\varnothing|$. Therefore, for a single round of the protocol,

$$\hat{o}_1(t_1)\hat{O}_1^\dagger = |1\rangle\langle 1| \hat{a}_{e,1}(t_1)\big(\sqrt{p_\parallel} \hat{A}_{e,1}^\dagger + \sqrt{p'_\perp p_\perp} \hat{A}_{e',1}^\dagger \hat{L}_1^\dagger \big)$$

$$+ |0\rangle\langle 0| \sqrt{p_\parallel} \hat{a}_1(t_1) \hat{A}_{l,1}^\dagger$$

$$+ |0\rangle\langle 1| \sqrt{p'_\perp p_\parallel} \hat{a}_{l,1}(t_1) \hat{A}_{l,1}^\dagger \hat{E}_1^\dagger. \tag{46}$$

Repeating the protocol N times with the initial spin state $|\Psi_0\rangle$, we arrive at

$$\langle\Psi_0|\,\hat{o}_1(t_1)\cdots\hat{o}_N(t_N)\hat{O}_N^\dagger\cdots\hat{O}_1^\dagger|\Psi_0\rangle$$

$$= \frac{1}{2}\Bigg[\prod_{j=1}^N \hat{a}_{e,j}(t_j)(\sqrt{p_\parallel}\hat{A}_{e,j}^\dagger + \sqrt{p'_\perp p_\perp}\hat{A}_{e',j}^\dagger\hat{L}_j^\dagger)$$

$$+ p_\parallel^{N/2}\Bigg(\prod_{j=1}^N\hat{a}_{l,j}(t_j)\hat{A}_{l,j}^\dagger + \sqrt{p'_\perp}\prod_{j=1}^N\hat{a}_{l,j}(t_j)\hat{A}_{l,j}^\dagger\hat{E}_j^\dagger\Bigg)\Bigg].$$

(47)

We now insert Eq. (47) and its Hermitian conjugate into (10) (for detailed derivations, see Appendix D) and arrive at the expression for the unconditional fidelity of the GHZ state,

$$\mathcal{F}_{\text{br}}^{(N)}[\text{GHZ}] = \frac{(p_\parallel + p'_\perp p_\perp)^N + p_\parallel^N(3 + p'_\perp)}{4}.$$

(48)

Since we reject the experimental outcomes where no photons have been detected, the final conditional fidelity (14) has to be normalized to the probability of detection $P(n_1 > 0, \ldots, n_N > 0)$ and becomes

$$\tilde{\mathcal{F}}_{\text{br}}^{(N)}[\text{GHZ}] = \frac{(p_\parallel + p'_\perp p_\perp)^N + p_\parallel^N(3 + p'_\perp)}{4P(n_1 > 0, \ldots, n_N > 0)}.$$

(49)

Each round of the protocol mixes the spin states due to the branching error, and the probability of detecting a photon in each of N rounds is not merely a product of individual probabilities. Instead, the success probability can be expanded as a product of conditional probabilities. Let $P(n_j, s = s_0)$ be a probability that a photon has been emitted and detected in jth round of the protocol with the spin ending in a state s_0. Then the following set of equations can be written:

$$P(n_1, \ldots, n_N) = P(n_1, \ldots, n_N, s = 0) + P(n_1, \ldots, n_N, s = 1) = (1 \quad 1)\begin{pmatrix} P(n_1, \ldots, n_N, s = 0) \\ P(n_1, \ldots, n_N, s = 1) \end{pmatrix}$$

$$= (1 \quad 1)\begin{pmatrix} P(n_N, s = 0|n_1, \ldots, n_{N-1}, s = 0)P(n_1, \ldots, n_{N-1}, s = 0) + P(n_N, s = 0|n_1, \ldots, n_{N-1}, s = 1)P(n_1, \ldots, n_{N-1}, s = 1) \\ P(n_N, s = 1|n_1, \ldots, n_{N-1}, s = 0)P(n_1, \ldots, n_{N-1}, s = 0) + P(n_N, s = 1|n_1, \ldots, n_{N-1}, s = 1)P(n_1, \ldots, n_{N-1}, s = 1) \end{pmatrix}$$

$$= (1 \quad 1)\begin{pmatrix} P(n_1, s = 0|n_1, \ldots, n_{N-1}, s = 0) & P(n_N, s = 0|n_1, \ldots, n_{N-1}, s = 1) \\ P(n_N, s = 1|n_1, \ldots, n_{N-1}, s = 0) & P(n_N, s = 1|n_1, \ldots, n_{N-1}, s = 1) \end{pmatrix}\begin{pmatrix} P(n_1, \ldots, n_{N-1}, s = 0) \\ P(n_1, \ldots, n_{N-1}, s = 1) \end{pmatrix}$$

$$= (1 \quad 1)\begin{pmatrix} M_{00} & M_{01} \\ M_{10} & M_{11} \end{pmatrix}\begin{pmatrix} P(n_1, \ldots, n_{N-1}, s = 0) \\ P(n_1, \ldots, n_{N-1}, s = 1) \end{pmatrix} = (1 \quad 1)M^N\begin{pmatrix} P(s = 0) \\ P(s = 1) \end{pmatrix} = (1 \quad 1)M^N\begin{pmatrix} 1/2 \\ 1/2 \end{pmatrix},$$

(50)

where the matrix M consists of the elements M_{ij} which are the probabilities to detect a photon while changing spin state from j to i between adjacent repetitions of the protocol. The elements of M can be derived by taking into account all possible processes in (44) that result in at least one photon detection,

$$M_{00} = p_\parallel, \quad M_{11} = p_\parallel + 2p_\perp p'_\perp + p_\perp^2, \quad M_{01} = p_\parallel(p_\perp + p'_\perp) + p'_\parallel p_\perp, \quad M_{10} = p_\perp.$$

(51)

Finally, we insert (48), (50), and (51) into Eq. (14) to obtain an expression for the conditional fidelity. Numerically calculated conditional fidelities for different number of photons are shown in Fig. 7.

The success probability (50) can be expanded up to the first order around a small parameter $p_{\text{wrong}}/p_\parallel \ll 1$ as

$$P^{(N)} = \frac{1}{2}(1 \quad 1)M^N\begin{pmatrix} 1 \\ 1 \end{pmatrix}$$

$$= \frac{p_\parallel^N}{2}(1 \quad 1)\Bigg[\hat{1} + \frac{1}{p_\parallel}\begin{pmatrix} 0 & p_\parallel(p_\perp + p'_\perp) + p_\perp p'_\parallel \\ p_\perp & p_\perp(p_\perp + 2p'_\perp) \end{pmatrix}\Bigg]^N\begin{pmatrix} 1 \\ 1 \end{pmatrix}$$

$$= p_\parallel^N\Bigg(1 + \frac{N}{2p_\parallel}[p_\parallel(p_\perp + p'_\perp) + p'_\parallel p_\perp + p_\perp(1 + p_\perp + 2p'_\perp)]\Bigg),$$

where p_{wrong} is any p other than $p_\parallel$. The conditional fidelity (14) to first order in $p_{\text{wrong}}/p_\parallel$ then becomes

$$\tilde{\mathcal{F}}^{(N)}[\text{GHZ}] = \frac{\mathcal{F}^{(N)}[\text{GHZ}]}{p_\parallel^N\{1 + \frac{N}{2p_\parallel}[p_\parallel(p_\perp + p'_\perp) + p'_\parallel p_\perp + p_\perp(1 + p_\perp + 2p'_\perp)]\}}$$

$$\approx \Bigg(1 + \frac{p'_\perp p_\parallel + Np'_\perp p_\perp}{4p_\parallel}\Bigg)\Bigg(1 - \frac{N}{2p_\parallel}[p_\parallel(p_\perp + p'_\perp) + p'_\parallel p_\perp + p_\perp(1 + p_\perp + 2p'_\perp)]\Bigg)$$

$$\approx 1 - N\frac{p_\perp(1 + p_\parallel) + p'_\parallel p_\perp + p_\parallel p'_\perp}{2p_\parallel} + \frac{p'_\perp}{4}.$$

(52)

FIG. 7. State fidelities with imperfect branching. Numerically calculated fidelities of the GHZ and cluster states are shown circles and dots, respectively. The solid lines show the first-order perturbative expressions for both the GHZ and the cluster states. Black and blue correspond to the fidelities with and without frequency filters, respectively. Here we use numerically simulated branching parameters for quantum dots embedded in a photonic crystal waveguide [52]: $\beta_\perp = 0.05$, $\beta'_\perp = 0.0025$, $\beta'_\parallel = 0.0025$, $\beta_\parallel = 1 - \beta_\perp - \beta'_\perp - \beta'_\parallel = 0.99$, corresponding to a branching ratio of $B \approx 140$.

As one can see from Fig. 7, the first-order approximation is accurate for few-photon GHZ states with high fidelity.

Next, we consider the typical experimental situation, where the collection efficiency is low and no frequency filtering is applied, which corresponds to $\eta_3 = \eta_2 = \eta$. Substituting (42) and (43) into Eq. (52) yields

$$\tilde{\mathcal{F}}^{(N)}_{\text{br,approx}}[\text{GHZ}] \approx 1 - N\left(\frac{3\beta_\perp + \beta'_\perp}{2}\right) + \frac{\beta'_\perp}{4}. \quad (53)$$

Frequency filters can be applied to suppress the contribution from the undesired diagonal transition, which corresponds to the creation operator $\hat{B}^\dagger$ in (15). Filtering the undesired photons can be accounted for by putting $\eta_3 \ll \eta_2 = \eta$, which then yields

$$\tilde{\mathcal{F}}^{(N)}_{\text{br,approx}}[\text{GHZ}] \approx 1 - N\frac{\beta_\perp + \beta'_\perp}{2} + \frac{\beta_\perp + \beta'_\perp}{4}$$
$$= 1 - \frac{1}{2(B+1)}\left(N - \frac{1}{2}\right), \quad (54)$$

where $B = (\beta_\parallel + \beta'_\parallel)/(\beta_\perp + \beta'_\perp)$ is the branching ratio between vertical and diagonal transitions in Fig. 2(d). As evident from Fig. 7, application of spectral filters improves the fidelity of the generated GHZ state with imperfect decay, which contrasts with the case of imperfect excitation (see Fig. 6).

2. Cluster state with branching errors

The calculation of the cluster-state fidelity with branching errors is similar to that of the GHZ state. Keeping only the terms that generate a correct cluster state, the single-round operator reads

$$\hat{O}^\dagger_j = |+\rangle \langle 1|(\sqrt{p_\parallel}\hat{A}^\dagger_{e,j} + \sqrt{p'_\perp p_\perp}\hat{A}^\dagger_{e',j}\hat{L}^\dagger_j)$$
$$+ |-\rangle \langle 0|\sqrt{p_\parallel}\hat{A}^\dagger_{l,j} + |-\rangle \langle 1|\sqrt{p'_\perp p_\parallel}\hat{A}^\dagger_{l,j}\hat{E}^\dagger_j\delta_{j,1}. \quad (55)$$

The first two processes correspond to the ideal operation of the protocol, while the other two produce the correct state due to the incorrect operation, i.e., via the diagonal transition. Furthermore, the Kronecker delta in the last term expresses the fact that only the first photon can produce the correct state when emitted in such process. Any other photon emitted in such process will results in a wrong spin-photon entangled state and hence will not contribute to the fidelity of the final state. As shown in Appendix D 2, the unconditional fidelity of the cluster state reads

$$\mathcal{F}^{(N)}_{\text{br}}[\text{Cl}] = \left(p_\parallel + \frac{p_\perp p'_\perp}{4}\right)^{N-1}\left(p_\parallel + \frac{p_\perp p'_\perp}{4} + \frac{p_\parallel p'_\perp}{4}\right). \quad (56)$$

The success probability $P(n_1 > 0, \ldots, n_N > 0)$ (50) is calculated analogously to the GHZ state with the matrix elements

$$M_{11} = M_{01} = \frac{p_\parallel + p_\perp^2 + p_\perp p_\parallel + p'_\perp p_\parallel + p_\perp p'_\parallel + 2p_\perp p'_\perp}{2},$$

$$M_{10} = M_{00} = \frac{1}{2}(p_\parallel + p_\perp).$$

Normalizing the fidelity (56) to the success probability yields the conditional fidelity shown in Fig. 7. In the first-order approximation, the fidelities of the cluster and GHZ state are identical and read

$$\tilde{\mathcal{F}}^{(N)}_{\text{br,approx}}[\text{Cl}] = \tilde{\mathcal{F}}^{(N)}_{\text{br,approx}}[\text{GHZ}]$$
$$\approx 1 - N\left(\frac{3\beta_\perp + \beta'_\perp}{2}\right) + \frac{\beta'_\perp}{4} \quad (57)$$

and

$$\tilde{\mathcal{F}}^{(N)}_{\text{br,approx}}[\text{Cl}] = \tilde{\mathcal{F}}^{(N)}_{\text{br,approx}}[\text{GHZ}]$$
$$\approx 1 - \left(N - \frac{1}{2}\right)\left(\frac{\beta_\perp + \beta'_\perp}{2}\right), \quad (58)$$

without and with the frequency filters, respectively. The difference of $\beta_\perp$ between the frequency-filtered and unfiltered output states can be understood by considering the difference between the effect of wrong photons emitted in the early and late time bins. With filtering, a diagonal transition in the late time bin does not create any photon and is thus removed by postselection. Bad effects thus appear only if the diagonal decay happens in the early time bin, followed by vertical decay in the late time bin. With filtering the wrong decay thus enters with only half the probability $(\beta_\perp + \beta'_\perp)/2$ (except if if happens in the first round where it disturbs only coherences and thus has half the effect, hence the factor of $N - 1/2$). Without filtering, however, also diagonal decays going into the waveguide in the late time bin will be accepted and early emissions on the diagonal transition will have twice the probability to be accepted since two photons are emitted in this case. Both of these effects result in the addition of the probability $\beta_\perp/2$.

C. Total fidelity and nature of the errors

Taking into account all error sources discussed above, we approximate the fidelity of the GHZ and cluster states by the
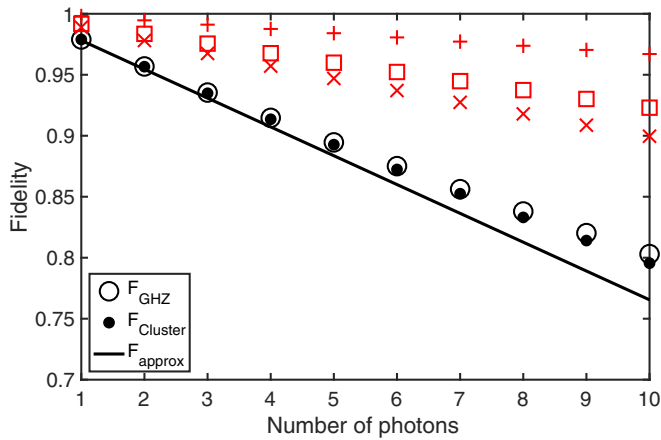
FIG. 8. Total fidelity versus number of photons with all imperfections and frequency filtering taken into account. Circles and dots show the fidelity of the GHZ and cluster states, respectively, and the solid line shows the first-order perturbative approximation of both states (60). Red symbols correspond to the different contributions in Eq. (59), namely, dephasing $\mathcal{F}_{\mathrm{ph}}$ ($\times$), excitation errors $\tilde{\mathcal{F}}_{\mathrm{exc}}$ ($\square$), and imperfect branching $\tilde{\mathcal{F}}_{\mathrm{br}}$ (+). Here $\Delta = 2\pi \times 64$ GHz, $\gamma_d = 0.06$ ns^{-1}, $\gamma_{\mathrm{opt}} = 5.3$ ns^{-1}, and β-factors are the same as in Fig. 7.

product of the individual fidelities,

$$\mathcal{F}_{\mathrm{GHZ/Cl}} = \mathcal{F}_{\mathrm{ph}} \times \tilde{\mathcal{F}}_{\mathrm{exc}} \times \tilde{\mathcal{F}}_{\mathrm{br}}. \tag{59}$$

Combining Eqs. (30), (41), and (58), the first-order analytical expression is equivalent for both states and reads

$$\mathcal{F}_{\mathrm{approx}} = 1 + \frac{1}{4(B+1)}$$
$$- N\left(\frac{\gamma_d}{\gamma + 2\gamma_d} + \frac{1}{2(B+1)} + \frac{\sqrt{3}\pi}{8}\frac{\gamma}{\Delta}\right). \tag{60}$$

Figure 8 shows the comparison between the full states fidelities and the first-order perturbative formula (60).

So far we have considered only the fidelity of the state, which gives a simple characterization of the quality of the state. The fidelity, however, reduces all imperfections to a single number and does not provide a full characterization of the complex many body state. More insight into the nature of the generated state can be obtained by further characterizing the nature of the errors occurring in the generation process.

The error arising from dephasing affects the coherence between the internal states $|0\rangle$ and $|1\rangle$ or equivalently the early and late time bins. This error can thus be characterised as a phase flip error acting on the spin qubit before the last rotation pulse $\hat{R}$, or on the emitted photon. The excitation error takes a similar form. In the limit where we have efficient filtering of off-resonant photons, the excitation errors conserve the logical basis states. This error can thus also be represented as the same phase flip. The branching error is more complicated. This process simultaneously affects the spin and the emitted photon. We analyze this situation more carefully in Appendix E, where we show that the dominant term from the branching error simultaneously affect two neighboring qubits.

A detailed understanding of nature of the error can be important for understanding potential applications of the states

towards more advanced applications. As a particular example Refs. [53–55] investigate the application of cluster states for universal quantum computation. Here different error thresholds are derived for models where single qubit errors are applied after the state preparation and for more detailed model that include initialization, entanglement, memory, and measurement errors. In the former model an error threshold of 3.2% (1.4%) per qubit are derived when computations are made with 3D (2D) cluster states. In Fig. 8 we use the realistic parameters for a QD-based emitter embedded in a photonic nanostructure [52]. Such systems are considered to be main candidates for producing streams of entangled photons due to simultaneously achievable high photon generation rates [50], good optical and spin coherence properties [50,56–58], near-perfect spin rotations [59], and a high internal efficiency β [60]. For the parameters of Figs. 7 and 8, the resulting infidelity per photon is 2.1%, which consists of 1.8% of single-qubit errors and 0.3% of two-qubit errors. The error is thus roughly comparable to those models and it is very encouraging that our estimates for current experimental parameters are of a similar magnitude as fault-tolerance requirements. Extending cluster states to two or three dimensions will of course introduce additional errors that are likely to reduce the quality of the produced states below the requirements for fault tolerance. Furthermore errors due to photon loss will also have to be accounted for. The exhaustive theoretical analysis conducted in this work, however, identifies the main bottlenecks and provides a clear pathway for improving further beyond what is currently possible in the experiments. A full assessment of higher-dimensional states is outside of the scope of this work and calls for further extensive theoretical investigation.

Finally, while fault-tolerant quantum computation is beyond reach of any currently available technology, the requirements for quantum communication tasks are typically much less stringent. The generated states are time-bin-entangled states of photons and thus ideally suited for quantum communication through optical fibers. Indeed the generated GHZ-states can be directly applied to anonymous transmission [61–63], secret sharing [30], and leader election [64]. Taking the anonymous transmission protocol [61–63] as an example, the error threshold is known to depends on the number of communicating parties. According to the security analysis of Ref. [61], the predicted error rates are within the threshold for up to at least 50 parties and almost an order of magnitude below the threshold for four parties.

V. CONCLUSION

In conclusion, we have developed a theoretical approach for assessing the fidelity of entangled photonic states produced by a single quantum emitter. We derive simple analytical expressions for evaluating the fidelity of the generated states. These expression provide a clear recipe for optimization of experimental parameters, such as photon emission rate and duration of the driving laser pulses. Our framework can be straightforwardly applied to a broad range of quantum emitters, including semiconductor QDs coupled to nanophotonic structures, defect centers in solids, and atoms in cavities. With the rapid experimental developments in

quantum nanophotonics we expect that these results can form the basis of near-future realizations of multiphoton emitters with a performance exceeding existing methods.

The considered time-bin generation protocol appears to be a particularly promising approach for the sequential production of entangled photons from quantum dot emitters (see also a more detailed discussion in Ref. [52]). Here it is highly appealing that our analysis shows that the output state is insensitive to a number of slow drifts of experimental parameters. Therefore, for instance, the very short T_2^* coherence time of spin qubits in quantum dots, which is a limiting factor in many quantum-information applications, does not compromise the protocol considered here. Based on our theoretical considerations, we predict that currently available quantum dot emitters can be used to produce five-photon GHZ and cluster states with fidelities of approximately 80%. A fidelity above the 50% level is present in states containing up to 10 subsequent photons. This is comparable to the state of the art achieved thus far with other methods [21,22], but the generation rate is expected to be much higher with the presented deterministic approach.

ACKNOWLEDGMENTS

APPENDIX A: IDEAL SCHEME FOR GENERATION OF THE CLUSTER STATE

Below we prove that the ideal scheme generates the cluster state for arbitrary large number of photons. Consider a single round of the protocol discussed in Sec. II, which can be written as

$$
\begin{aligned}
\hat{O}^\dagger = \hat{H}\hat{L}^\dagger\hat{X}\hat{E}^\dagger &= \frac{1}{\sqrt{2}}((|0\rangle + |1\rangle)\langle 0| + (|0\rangle - |1\rangle)\langle 1|) \\
&\times (|0\rangle\langle 0| + |1\rangle\langle 1|\hat{a}_l^\dagger)(|0\rangle\langle 1| + |1\rangle\langle 0|) \\
&\times (|0\rangle\langle 0| + |1\rangle\langle 1|\hat{a}_e^\dagger) \\
&= \frac{1}{\sqrt{2}}(|0\rangle + |1\rangle)\langle 1|\hat{a}_e^\dagger + \frac{1}{\sqrt{2}}(|0\rangle - |1\rangle)\langle 0|\hat{a}_l^\dagger, \quad \text{(A1)}
\end{aligned}
$$

where $\hat{E}^\dagger$ and $\hat{L}^\dagger$ are, respectively, the operators corresponding to the generations of an early and a late photons. For convenience, let us change basis and choose the logical spin states as $|0\rangle \rightarrow |1\rangle$, $|1\rangle \rightarrow |0\rangle$ and the logical photon states as $\hat{a}_e^\dagger \rightarrow \hat{a}_0^\dagger$, $\hat{a}_l^\dagger \rightarrow -\hat{a}_1^\dagger$, thus turning the operator of Eq. (A1) into

$$
\hat{O}^\dagger = |+\rangle\langle 0|\hat{a}_0^\dagger + |-\rangle\langle 1|\hat{a}_1^\dagger, \quad \text{(A2)}
$$

where $\hat{a}_0^\dagger$ and $\hat{a}_1^\dagger$ create photons in states $|0\rangle$ and $|1\rangle$, respectively, and $|\pm\rangle = (|0\rangle \pm |1\rangle)/\sqrt{2}$. By definition, an $(N+1)$-qubit cluster state is a simultaneous eigenstate of the

operators $\hat{g}_i$, where

$$
\begin{aligned}
\hat{g}_i &= \hat{Z}_{i-1}\hat{X}_i\hat{Z}_{i+1} \; \forall i = [1, N-1], \\
\hat{g}_0 &= \hat{X}_0\hat{Z}_1, \quad \hat{g}_N = \hat{Z}_{N-1}\hat{X}_N, \quad \text{(A3)}
\end{aligned}
$$

with $\hat{Z}$ and $\hat{X}$ being the Pauli-Z and Pauli-X matrices, respectively. We will now prove the following theorem:

Theorem. Assume that $|\Psi_N\rangle$ is a cluster state generated by the action of the operator $\hat{O}^\dagger$ (A2), such that $g_i = 1 \; \forall \; i = [0, N]$. Then the state $|\Psi_{N+1}\rangle = \hat{O}^\dagger |\Psi_N\rangle$ is also a cluster state with $g_i = 1 \; \forall \; i = [0, N+1]$.

Proof. We start by writing the operator $\hat{O}^\dagger$ from (A2) in two bases,

$$
\hat{O}^\dagger_{x \leftarrow z} = |+\rangle\hat{a}_0^\dagger\langle 0| + |-\rangle\hat{a}_1^\dagger\langle 1| \quad \text{(A4)}
$$

and

$$
\begin{aligned}
\hat{O}^\dagger_{z \leftarrow x} &= \frac{1}{\sqrt{2}}(|0\rangle\hat{a}_+^\dagger + |1\rangle\hat{a}_-^\dagger)\langle +| \\
&+ \frac{1}{\sqrt{2}}(|0\rangle\hat{a}_-^\dagger + |1\rangle\hat{a}_+^\dagger)\langle -|, \quad \text{(A5)}
\end{aligned}
$$

where $\hat{a}_\pm = (\hat{a}_0 \pm \hat{a}_1)/\sqrt{2}$.

Since the cluster state is an eigenstate of $\hat{g}_N$ and $\hat{g}_{N-1}$, the general form of the state $|\Psi_N\rangle$ can be written in each of the two bases,

$$
\left|\Psi_N^{(xz)}\right\rangle = |+0\rangle\left|\Psi_{N-2}^{(+0)}\right\rangle + |-1\rangle\left|\Psi_{N-2}^{(-1)}\right\rangle \quad \text{(A6)}
$$

and

$$
\begin{aligned}
\left|\Psi_N^{(zx)}\right\rangle &= |0+0\rangle\left|\Psi_{N-3}^{(0+0)}\right\rangle + |1-0\rangle\left|\Psi_{N-3}^{(1-0)}\right\rangle \\
&+ |0-1\rangle\left|\Psi_{N-3}^{(0-1)}\right\rangle + |1+1\rangle\left|\Psi_{N-3}^{(1+1)}\right\rangle, \quad \text{(A7)}
\end{aligned}
$$

where we label the spin-photon states such that the spin state is always the ket-vector furthest to the left followed by the photon states, i.e., $|\Psi_N\rangle = |\text{Spin}, \text{Photon}_N, \text{Photon}_{N-1}, \ldots\rangle$.

To prove that the state $|\Psi_{N+1}\rangle$ is a cluster state, we need to show that all stabilizers obey $g_i = 1 \; \forall \; i = [0, N+1]$. The operator $\hat{O}^\dagger$ acts only on the qubit no. N and adds the qubit no. $(N+1)$. Thus, it does not change the value of the stabilizers g_1 to g_{N-2} and it suffices to prove that the eigenvalues of the stabilizers $\hat{g}_{N-1}$, $\hat{g}_N$, and $\hat{g}_{N+1}$ are equal to 1. First, we act with the operator $\hat{O}^\dagger_{x \leftarrow z}$ (A4) on the state $|\Psi_N^{(zx)}\rangle$ (A7),

$$
\begin{aligned}
\left|\Psi_{N+1}^{xz}\right\rangle &= \hat{O}^\dagger_{x \leftarrow z}\left|\Psi_N^{(zx)}\right\rangle \\
&= |+0+0\rangle\left|\Psi_{N-3}^{(0+0)}\right\rangle + |-1-0\rangle\left|\Psi_{N-3}^{(1-0)}\right\rangle \\
&+ |+0-1\rangle\left|\Psi_{N-3}^{(0-1)}\right\rangle + |-1+1\rangle\left|\Psi_{N-3}^{(1+1)}\right\rangle. \quad \text{(A8)}
\end{aligned}
$$

From the second line of the equation above it follows that the $g_{N+1} = 1$ and $g_{N-1} = 1$.

Next, we act with the operator $\hat{O}^\dagger_{z \leftarrow x}$ (A5) on the state $|\Psi_N^{(xz)}\rangle$ (A6),

$$
\begin{aligned}
\left|\Psi_{N+1}^{zx}\right\rangle &= \hat{O}^\dagger_{z \leftarrow x}\left|\Psi_N^{(xz)}\right\rangle \\
&= |0+0\rangle\left|\Psi_{N-2}^{+0}\right\rangle + |1-0\rangle\left|\Psi_{N-2}^{-0}\right\rangle \\
&+ |0-1\rangle\left|\Psi_{N-2}^{-1}\right\rangle + |1+1\rangle\left|\Psi_{N-2}^{+1}\right\rangle. \quad \text{(A9)}
\end{aligned}
$$

Therefore, the state $|\Psi_{N+1}^{zx}\rangle$ obeys $g_N = 1$ and we have proven that all stabilizers obey $g_i = 1$. Thus, an operator $\hat{O}^\dagger$ takes an N-qubit cluster state to an $(N + 1)$-qubit cluster state. This concludes the proof of the theorem. ∎

To complete the proof that the procedure creates a cluster state we still need to show that we can generate a cluster state for a small N. This can be proven by applying the operator $\hat{O}^\dagger$

of Eq. (A2) twice to a qubit initially prepared in $|\Psi_0\rangle = |+\rangle$, which produces a state

$$
\begin{aligned}
|\Psi_2\rangle = \hat{O}_2^\dagger \hat{O}_1^\dagger |\Psi_0, \emptyset\rangle &= \frac{1}{\sqrt{2}}(|+0+\rangle + |-1-\rangle) \\
&= \frac{1}{2}(|0+0\rangle + |1+1\rangle + |0-1\rangle + |1-0\rangle).
\end{aligned} \tag{A10}
$$

This state can be directly verified to be a cluster state.

APPENDIX B: FIDELITIES OF NON-SPIN-MIXING ERRORS

1. GHZ state

The N-photon operators that enter the expression for the operational fidelity (10) read

$$
\hat{o}_1 \cdots \hat{o}_N \hat{O}_N^\dagger \cdots \hat{O}_1^\dagger = |1\rangle\langle 1| \hat{a}_{e,1}(t_1) \hat{A}_{e,1}^\dagger \cdots \hat{a}_{e,N}(t_N) \hat{A}_{e,N}^\dagger + |0\rangle\langle 0| \hat{a}_{l,1}(t_1) \hat{A}_{l,1}^\dagger \cdots \hat{a}_{l,N}(t_N) \hat{A}_{l,N}^\dagger. \tag{B1}
$$

Inserting (B1) and its Hermitian conjugate into equation for the operational fidelity (10), we obtain

$$
\begin{aligned}
\mathcal{F}^{(N)}[\text{GHZ}] = \text{Tr}_{\text{env}} \Bigg\{ &\int_0^\infty dt_N \cdots \int_0^\infty dt_1 \langle\emptyset|\langle\Psi_0| \left(|1\rangle\langle 1| \hat{a}_{e,1}(t_1)\hat{A}_{e,1}^\dagger \cdots \hat{a}_{e,N}(t_N)\hat{A}_{e,N}^\dagger + |0\rangle\langle 0| \hat{a}_{l,1}(t_1)\hat{A}_{l,1}^\dagger \cdots \hat{a}_{l,N}(t_N)\hat{A}_{l,N}^\dagger \right) \\
&|\Psi_0\rangle |\emptyset\rangle \langle\emptyset|\langle\Psi_0| \left(|1\rangle\langle 1| \hat{A}_{e,1}\hat{a}_{e,1}^\dagger(t_1) \cdots \hat{A}_{e,N}\hat{a}_{e,N}^\dagger(t_N) + |0\rangle\langle 0| \hat{A}_{l,1}\hat{a}_{l,1}^\dagger(t_1) \cdots \hat{A}_{l,N}\hat{a}_{l,N}^\dagger(t_N) \right) |\Psi_0\rangle |\emptyset\rangle \\
= \frac{1}{4}\text{Tr}_{\text{env}} \Bigg\{ &\int_0^\infty dt_N \cdots \int_0^\infty dt_1 \langle\emptyset| \left(\hat{a}_{e,1}(t_1)\hat{A}_{e,1}^\dagger \cdots \hat{a}_{e,N}(t_N)\hat{A}_{e,N}^\dagger + \hat{a}_{l,1}(t_1)\hat{A}_{l,1}^\dagger \cdots \hat{a}_{l,N}(t_N)\hat{A}_{l,N}^\dagger \right) |\emptyset\rangle \\
&\langle\emptyset| \left(\hat{A}_{e,1}\hat{a}_{e,1}^\dagger(t_1) \cdots \hat{A}_{e,N}\hat{a}_{e,N}^\dagger(t_N) + \hat{A}_{l,1}\hat{a}_{l,1}^\dagger(t_1) \cdots \hat{A}_{l,N}\hat{a}_{l,N}^\dagger(t_N) \right) |\emptyset\rangle \Bigg\} \\
= \frac{1}{4}\text{Tr}_{\text{env}} \Bigg\{ &\int_0^\infty dt_N \cdots \int_0^\infty dt_1 \langle\emptyset| \left(\hat{a}_{e,1}(t_1)\hat{A}_{e,1}^\dagger \cdots \hat{a}_{e,N}(t_N)\hat{A}_{e,N}^\dagger |\emptyset\rangle \langle\emptyset| \hat{A}_{e,1}\hat{a}_{e,1}^\dagger(t_1) \cdots \hat{A}_{e,N}\hat{a}_{e,N}^\dagger(t_N) \right) |\emptyset\rangle \\
&+ \int_0^\infty dt_N \cdots \int_0^\infty dt_1 \langle\emptyset| \left(\hat{a}_{l,1}(t_1)\hat{A}_{l,1}^\dagger \cdots \hat{a}_{l,N}(t_N)\hat{A}_{l,N}^\dagger |\emptyset\rangle \langle\emptyset| \hat{A}_{e,1}\hat{a}_{e,1}^\dagger(t_1) \cdots \hat{A}_{e,N}\hat{a}_{e,N}^\dagger(t_N) \right) |\emptyset\rangle \\
&+ \int_0^\infty dt_N \cdots \int_0^\infty dt_1 \langle\emptyset| \left(\hat{a}_{e,1}(t_1)\hat{A}_{e,1}^\dagger \cdots \hat{a}_{e,N}(t_N)\hat{A}_{e,N}^\dagger |\emptyset\rangle \langle\emptyset| \hat{A}_{l,1}\hat{a}_{l,1}^\dagger(t_1) \cdots \hat{A}_{l,N}\hat{a}_{l,N}^\dagger(t_N) \right) |\emptyset\rangle \\
&+ \int_0^\infty dt_N \cdots \int_0^\infty dt_1 \langle\emptyset| \left(\hat{a}_{l,1}(t_1)\hat{A}_{l,1}^\dagger \cdots \hat{a}_{l,N}(t_N)\hat{A}_{l,N}^\dagger |\emptyset\rangle \langle\emptyset| \hat{A}_{l,1}\hat{a}_{l,1}^\dagger(t_1) \cdots \hat{A}_{l,N}\hat{a}_{l,N}^\dagger(t_N) \right) |\emptyset\rangle \Bigg\} \\
= \frac{1}{4}\text{Tr}_{\text{env}} &\sum_{u,v=e,l} \left(\int_0^\infty dt \langle\emptyset| \hat{a}_u(t)\hat{A}_u^\dagger |\emptyset\rangle \langle\emptyset| \hat{A}_v \hat{a}_v^\dagger(t) |\emptyset\rangle \right)^N.
\end{aligned} \tag{B2}
$$

In the last step we have used that the photonic operators $\hat{A}_u$ for different time periods commute. This means that the photonic part of the matrix element can be separated into products. Note, however, that the operators $\hat{A}_u^\dagger$ may contain couplings to different degrees of freedom, for which this factorization may not be the applicable, e.g., in Sec. IV A 2, $\hat{A}_u^\dagger$ contain the coupling to a phononic environment. In this case the Nth order product of $\hat{A}_u^\dagger$ operators should in principle be evaluated as a suitable time-ordered product for different periods. We will, however, consider only situations in which this product can be completely separated, e.g., a Markovian phononic reservoir.

In general the approximation applied here is reminiscent of the Markovian approximation often employed in quantum optics, but not exactly the same. In particular slowly varying classical parameters as considered in Sec. IV A 1 do not fit into the usual Markovian approximation, but is still compatible with (B2), provided that the average over the classical parameter (implied by Tr_{env}) is performed for the final Nth-order product and not for each term individually. On the other hand, the situation would be more complicated if we were, e.g., considering a non-Markovian phononic reservoir.

2. Cluster state

For the cluster state the two-photon operator is

$$\hat{o}_1(t_1)\hat{o}_2(t_2)\hat{O}_2^\dagger\hat{O}_1^\dagger = (|1\rangle\langle0|\,\hat{a}_{e,1}(t_1) + |0\rangle\langle1|\,\hat{a}_{l,1}(t_1))\hat{H}^\dagger(|1\rangle\langle1|\,\hat{a}_{e,2}(t_2)\hat{A}_{e,2}^\dagger + |0\rangle\langle0|\,\hat{a}_{l,2}(t_2)\hat{A}_{l,2}^\dagger)\hat{H}(|0\rangle\langle1|\,\hat{A}_{e,1}^\dagger + |1\rangle\langle0|\,\hat{A}_{l,1}^\dagger)$$

$$= \frac{1}{2}\big[\,|1\rangle\langle1|\,\hat{a}_{e,1}(t_1)\hat{A}_{e,1}^\dagger \otimes (\hat{a}_{e,2}(t_2)\hat{A}_{e,2}^\dagger + \hat{a}_{l,2}(t_2)\hat{A}_{l,2}^\dagger) + |1\rangle\langle1|\,\hat{a}_{l,1}(t_1)\hat{A}_{l,1}^\dagger \otimes (\hat{a}_{e,2}(t_2)\hat{A}_{e,2}^\dagger + \hat{a}_{l,2}(t_2)\hat{A}_{l,2}^\dagger)\big]$$

$$= \frac{1}{2}(|1\rangle\langle1|\,\hat{a}_{e,1}(t_1)\hat{A}_{e,1}^\dagger + |0\rangle\langle0|\,\hat{a}_{l,1}(t_1)\hat{A}_{l,1}^\dagger) \otimes (\hat{a}_{e,2}(t_2)\hat{A}_{e,2}^\dagger + \hat{a}_{l,2}(t_2)\hat{A}_{l,2}^\dagger), \tag{B3}$$

where we have omitted cross-terms such as $\hat{a}_{l,1}(t_1)\hat{a}_{l,2}(t_2)\hat{A}_{l,2}^\dagger\hat{A}_{e,1}^\dagger$ since they will vanish when sandwiched with the photon vacuum, $\langle\emptyset_1|\,\hat{a}_{l,1}(t_1)\hat{A}_{e,1}^\dagger\,|\emptyset_1\rangle = 0$. For arbitrary N, this generalizes to

$$\hat{o}_1(t_1)\cdots\hat{o}_N(t_N)\hat{O}_N^\dagger\cdots\hat{O}_1^\dagger = \frac{1}{2^{N-1}}(|1\rangle\langle1|\,\hat{a}_{e,1}(t_1)\hat{A}_{e,1}^\dagger + |0\rangle\langle0|\,\hat{a}_{l,1}(t_1)\hat{A}_{l,1}^\dagger) \otimes \prod_{j=2}^N (\hat{a}_{e,j}(t_j)\hat{A}_{e,j}^\dagger + \hat{a}_{l,j}(t_j)\hat{A}_{l,j}^\dagger), \tag{B4}$$

and applying it to the initial spin state $|\Psi_0\rangle = (|0\rangle + |1\rangle)/\sqrt{2}$ we find

$$\langle\Psi_0|\,\hat{o}_1(t_1)\cdots\hat{o}_N(t_N)\hat{O}_N^\dagger\cdots\hat{O}_1^\dagger\,|\Psi_0\rangle = \frac{1}{2^N}\prod_{j=1}^N (\hat{a}_{e,j}(t_j)\hat{A}_{e,j}^\dagger + \hat{a}_{l,j}(t_j)\hat{A}_{l,j}^\dagger). \tag{B5}$$

Substituting (B5) into (10), one arrives at

$$\mathcal{F}^{(N)}[\text{Cl}] = \text{Tr}_{\text{env}}\int_0^\infty dt_N\cdots\int_0^\infty dt_1\,\langle\emptyset|\langle\Psi_0|\,\hat{o}_1(t_1)\cdots\hat{o}_N(t_N)\hat{O}_N^\dagger\cdots\hat{O}_1^\dagger\,|\Psi_0\rangle|\emptyset\rangle\langle\emptyset|\langle\Psi_0|\,\hat{O}_1\cdots\hat{O}_N\hat{o}_N^\dagger(t_N)\cdots\hat{o}_1^\dagger(t_1)\,|\Psi_0\rangle|\emptyset\rangle$$

$$= \frac{1}{2^{2N}}\text{Tr}_{\text{env}}\int_0^\infty dt_N\cdots\int_0^\infty dt_1\,\langle\emptyset|\prod_{j=1}^N(\hat{a}_{e,j}(t_j)\hat{A}_{e,j}^\dagger + \hat{a}_{l,j}(t_j)\hat{A}_{l,j}^\dagger)|\emptyset\rangle\langle\emptyset|\,(\hat{A}_{e,j}\hat{a}_{e,j}^\dagger(t_j) + \hat{A}_{l,j}\hat{a}_{l,j}^\dagger(t_j))\,|\emptyset\rangle$$

$$= \frac{1}{2^{2N}}\text{Tr}_{\text{env}}\int_0^\infty dt_1\,\langle\emptyset_1|\,(\hat{a}_{e,1}(t_1)\hat{A}_{e,1}^\dagger + \hat{a}_{l,1}(t_1)\hat{A}_{l,1}^\dagger)\,|\emptyset_1\rangle\langle\emptyset_1|\,(\hat{A}_{e,1}\hat{a}_{e,1}^\dagger(t_1) + \hat{A}_{l,1}\hat{a}_{l,1}^\dagger(t_1))\,|\emptyset_1\rangle \times \cdots$$

$$\times \int_0^\infty dt_N\,\langle\emptyset_N|\,(\hat{a}_{e,N}(t_N)\hat{A}_{e,N}^\dagger + \hat{a}_{l,N}(t_N)\hat{A}_{l,N}^\dagger)\,|\emptyset_N\rangle\langle\emptyset_N|\,(\hat{A}_{e,N}\hat{a}_{e,N}^\dagger(t_N) + \hat{A}_{l,N}\hat{a}_{l,N}^\dagger(t_N))\,|\emptyset_N\rangle$$

$$= \text{Tr}_{\text{env}}\left(\frac{1}{4}\sum_{u,v=e,l}\int_0^\infty dt\,\langle\emptyset|\,\hat{a}_u(t)\hat{A}_u^\dagger\,|\emptyset\rangle\langle\emptyset|\,\hat{A}_v\hat{a}_v^\dagger(t)\,|\emptyset\rangle\right)^N. \tag{B6}$$

In the last step we have again applied the approximation discussed after Eq. (B2).

APPENDIX C: TWO-PHOTON EMISSIONS

We are interested in taking into account the action of the temporal and frequency filters on the output state (33).

1. Frequency filters

For convenience, we start from frequency filtering. Applying the transformation in Eq. (15), the creation operators (35) become

$$\hat{\tilde{Q}}_{u,j}^\dagger = \big(c_1 + c_2\sqrt{\eta_2}\hat{A}_0^{\dagger,u} + c_2(1-\sqrt{\eta_2})\hat{\tilde{A}}_0^{\dagger,u}\Phi_1\hat{A}_{p_1}^{\dagger,u} + \Phi_2\sqrt{\eta_2}\hat{A}_{p_2}^{\dagger,u}\hat{A}_0^{\dagger,u} + \Phi_2\sqrt{1-\eta_2}\hat{A}_{p_2}^{\dagger,u}\hat{\tilde{A}}_0^{\dagger,u}\big)_j$$

$$\times \big(c_1 + c_2\sqrt{\eta_3}\hat{B}_0^{\dagger,v} + c_2(1-\sqrt{\eta_3})\hat{\tilde{B}}_0^{\dagger,v}\Phi_1\hat{A}_{p_1}^{\dagger,v} + \Phi_2\sqrt{\eta_3}\hat{B}_{p_2}^{\dagger,v}\hat{B}_0^{\dagger,v} + \Phi_2\sqrt{1-\eta_3}\hat{B}_{p_2}^{\dagger,v}\hat{\tilde{B}}_0^{\dagger,v}\big)_j, \tag{C1}$$

where j is the photon number and $\{u,v\} = \{e,l\}$, $u \neq v$.

2. Temporal filters

We condition on detecting a photon in the decay period of either the early or the late pulse. We thus apply the projector $\hat{P}_{n_{0j}>0}$ on the operator above thus keeping only the terms that correspond to receiving at least one photon after each excitation pulse,

$$\hat{P}_{n_{0j}>0}\hat{\tilde{Q}}_{u,j}^\dagger = c_1c_3\sqrt{\eta_3}\hat{B}_0^{\dagger,v} + c_1\Phi_3\sqrt{\eta_3}\hat{B}_0^{\dagger,v}\hat{B}_{p_2}^{\dagger,v} + c_2c_0\sqrt{\eta_2}\hat{A}_0^{\dagger,u} + c_2\Phi_3\sqrt{\eta_2}\sqrt{\eta_3}\hat{A}_0^{\dagger,u}\hat{B}_0^{\dagger,v} + c_2c_3\sqrt{\eta_2}\sqrt{1-\eta_3}\hat{A}_0^{\dagger,u}\hat{B}_0^{\dagger,v}$$

$$+ c_2\Phi_0\sqrt{\eta_2}\hat{A}_0^{\dagger,u}\hat{B}_{p_1}^{\dagger,v} + c_2\Phi_3\sqrt{\eta_2}\sqrt{\eta_3}\hat{A}_0^{\dagger,u}\hat{B}_{p_2}^{\dagger,v}\hat{B}_0^{\dagger,v} + c_2\Phi_3\sqrt{\eta_2}\sqrt{1-\eta_3}\hat{A}_0^{\dagger,u}\hat{B}_{p_2}^{\dagger,v}\hat{\tilde{B}}_0^{\dagger,v} + c_2c_3\sqrt{\eta_3}\sqrt{1-\eta_2}\hat{\tilde{A}}_0^{\dagger,u}\hat{B}_0^{\dagger,v}$$

$$+ c_2\Phi_3\sqrt{\eta_3}\sqrt{1-\eta_2}\hat{A}_0^{\dagger,u}\hat{B}_{p_2}^{\dagger,v}\hat{B}_0^{\dagger,v} + c_3\Phi_1\sqrt{\eta_3}\hat{A}_{p_1}^{\dagger,u}\hat{B}_0^{\dagger,v} + \Phi_1\Phi_3\sqrt{\eta_3}\hat{A}_{p_1}^{\dagger,u}\hat{B}_{p_2}^{\dagger,v}\hat{B}_0^{\dagger,v} + \Phi_2 c_0\sqrt{\eta_2}\hat{A}_{p_2}^{\dagger,u}\hat{A}_0^{\dagger,u}$$

$$+ \Phi_2 c_3\sqrt{\eta_2}\sqrt{\eta_3}\hat{A}_{p_2}^{\dagger,u}\hat{A}_0^{\dagger,u}\hat{B}_0^{\dagger,v} + \Phi_2 c_3\sqrt{\eta_2}\sqrt{1-\eta_3}\hat{A}_{p_2}^{\dagger,u}\hat{A}_0^{\dagger,u}\hat{B}_0^{\dagger,v} + \Phi_2\Phi_0\sqrt{\eta_2}\hat{A}_{p_2}^{\dagger,u}\hat{A}_0^{\dagger,u}\hat{B}_0^{\dagger,v}$$

$$+ \Phi_2\Phi_3\sqrt{\eta_2}\sqrt{\eta_3}\hat{A}_{p_2}^{\dagger,u}\hat{A}_0^{\dagger,u}\hat{B}_0^{\dagger,v}\hat{B}_{p_2}^{\dagger,v} + \Phi_2\Phi_3\sqrt{\eta_2}\sqrt{1-\eta_3}\hat{A}_{p_2}^{\dagger,u}\hat{A}_0^{\dagger,u}\hat{B}_0^{\dagger,v}\hat{B}_{p_2}^{\dagger,v}$$

$$+ \Phi_2 c_3\sqrt{1-\eta_2}\sqrt{\eta_3}\hat{A}_{p_2}^{\dagger,u}\hat{A}_0^{\dagger,u}\hat{B}_0^{\dagger,v} + \Phi_2\Phi_3\sqrt{1-\eta_2}\sqrt{\eta_3}\hat{A}_{p_2}^{\dagger,u}\hat{A}_0^{\dagger,u}\hat{B}_0^{\dagger,v}\hat{B}_{p_2}^{\dagger,v}. \tag{C2}$$

3. Conditional fidelity

We can now calculate the fidelities (16) and (17), with the photons emitted during the excitation sequence playing a role of the environment. Since the photons emitted in different time bins are orthogonal, the only off-diagonal terms in (16) and (17) which survive the trace operation are

$$\text{Tr}_{\text{pulse}} \int_0^\infty dt \, \langle\emptyset| \hat{a}_u(t)\hat{P}_{n>0}\hat{\hat{Q}}_u^{\dagger}|\emptyset\rangle \, \langle\emptyset|(\hat{P}_{n>0}\hat{\hat{Q}}_v^{\dagger})^\dagger \hat{a}_v^\dagger(t)|\emptyset\rangle$$

$$= \int_0^\infty dt \, \langle\emptyset| \hat{a}_u(t)\hat{P}_{n>0}\big(c_1 c_3\sqrt{\eta_3}\hat{B}_0^{\dagger,v} + c_0 c_2\sqrt{\eta_2}\hat{A}_0^{\dagger,u}\big)|\emptyset\rangle \, \langle\emptyset|(c_1 c_3\sqrt{\eta_3}\hat{B}_0^{\dagger,u} + c_0 c_2\sqrt{\eta_2}\hat{A}_0^{\dagger,v})^\dagger \hat{a}_v^\dagger(t)|\emptyset\rangle = \eta_2|c_0 c_2|^2. \tag{C3}$$

The diagonal terms will contain contribution from all terms that include $\hat{A}_0^\dagger$ in (C2). Since none of these terms interfere, the diagonal terms is given by the sum of the corresponding coefficients square,

$$\text{Tr}_{\text{pulse}} \int_0^\infty dt \, \langle\emptyset| \hat{a}_u(t)\hat{P}_{n>0}\hat{\hat{Q}}_u^{\dagger}|\emptyset\rangle \, \langle\emptyset|(\hat{P}_{n>0}\hat{\hat{Q}}_u^{\dagger})^\dagger \hat{a}_u^\dagger(t)|\emptyset\rangle$$

$$= \eta_2(|c_0 c_2|^2 + |c_0\Phi_2|^2 + |c_2\Phi_0|^2 + |\Phi_0\Phi_2|^2) + \eta_2(1-\eta_3)(|c_3 c_2|^2 + |c_3\Phi_2|^2 + |c_2\Phi_3|^2 + |\Phi_2\Phi_3|^2). \tag{C4}$$

Finally, for the calculation of the detection probability all terms in (C2) contribute and none of the terms interfere, therefore the success probability is given by the sum of the square of all coefficients in (C2) and becomes (38).

4. Calculations of the wave-function coefficients

In order to obtain an expression for the conditional fidelity affected by imperfect excitation process, we need to calculate all the coefficients in (35). Following a wave-function ansatz method of Ref. [43] and after some algebra, the coupled differential equations for the first-order coefficients become

$$\frac{\partial}{\partial\tau}c_e(\tau) = i\frac{\tilde{\Omega}}{2}c_g(\tau) - \left(\frac{1}{2} + i\tilde{\Delta}\right)c_e(\tau), \quad \frac{\partial}{\partial\tau}c_g(\tau) = i\frac{\tilde{\Omega}}{2}c_e(\tau), \quad c_e(0) = 0, \quad c_g(0) = 1, \tag{C5}$$

while the second-order coefficients are governed by

$$\phi_g(\tau, \tau_e) = ie^{-i\tilde{\Delta}\tau}c_e(\tau_e)\theta(\tau_e - \tau), \quad \phi_e(\tau, \tau_e) = 0 \tag{C6}$$

for $\tau < \tau_e$ and

$$\frac{\partial}{\partial\tau}\phi_e(\tau, \tau_e) = i\frac{\tilde{\Omega}}{2}\phi_g(\tau, \tau_e) - \left(\frac{1}{2} + i\tilde{\Delta}\right)\phi_e(\tau, \tau_e),$$

$$\frac{\partial}{\partial\tau}\phi_g(\tau, \tau_e) = i\frac{\tilde{\Omega}}{2}\phi_e(\tau, \tau_e), \quad \phi_g(\tau_e, \tau_e) = ie^{-i\tilde{\Delta}\tau_e}c_e(\tau_e), \quad \phi_e(\tau_e, \tau_e) = 0 \tag{C7}$$

for $\tau > \tau_e$, respectively. The dimensionless units used above are $\tau = \gamma t$, $\tilde{\Delta} = \Delta/\gamma$, and $\tilde{\Omega} = \Omega/\gamma$. The equations above have been analytically solved in first-order perturbation theory for a square-shaped pulse in Ref. [51]. Adjusting the square pulse to the optimal duration $T_{\text{opt,sq}} = \sqrt{3}\pi/\Delta$, which ensures that a 2π Rabi oscillation has been performed on the off-resonant transition, while the the resonant transition performs a π rotation, the wave-function coefficients read

$$|c_3|^2 = 0, \quad |c_0|^2 = 1, \quad |c_1|^2 = \frac{\sqrt{3}\pi}{2\tilde{\Delta}}, \quad |c_2|^2 = 1 - \frac{\sqrt{3}\pi}{2\tilde{\Delta}},$$

$$|\Phi_2|^2 = \frac{\sqrt{3}\pi}{8\tilde{\Delta}}\left(1 - \frac{\sqrt{3}\pi}{2\tilde{\Delta}}\right), \quad |\Phi_1|^2 = \frac{3\sqrt{3}\pi}{8\tilde{\Delta}} - \frac{3\pi^2}{2\tilde{\Delta}^2}\left(\frac{3}{8} - \frac{1}{\pi^2}\right),$$

$$|\Phi_3|^2 = \frac{3}{16}\left(\frac{\sqrt{3}\pi}{8\tilde{\Delta}} - \frac{3\pi^2}{16\tilde{\Delta}^2}\right), \quad |\Phi_0|^2 = \frac{13\sqrt{3}\pi}{128\tilde{\Delta}}\left(1 - \frac{\sqrt{3}\pi}{2\tilde{\Delta}}\right). \tag{C8}$$

Inserting these coefficients into Eq. (40) and expanding up to the first order in γ/Δ, we arrive at an expression for the fidelities of both the GHZ and the cluster states

$$\tilde{\mathcal{F}}_{\text{exc,sq}} = 1 - \frac{N\gamma\sqrt{3}\pi}{256\Delta}\left(29 + 3\left[1 + \frac{\xi_3}{\xi_2}\right]\right). \tag{C9}$$

With perfect frequency filters $\xi_2 = 1$, $\xi_3 = 0$, this turns into

$$\tilde{\mathcal{F}}_{\text{exc,sq}} = 1 - N\frac{\gamma\sqrt{3}\pi}{8\Delta}. \tag{C10}$$

APPENDIX D: FIDELITIES OF THE STATES WITH BRANCHING ERRORS

1. GHZ state with branching error

Substituting (47) and its Hermitian conjugate into Eq. (10) yields

$$\mathcal{F}^{(N)} = \text{Tr}_{\text{photons}}\left\{ \int_0^\infty dt_N \cdots \int_0^\infty dt_1 \langle \emptyset | \langle \Psi_0 | \hat{o}_1(t_1) \cdots \hat{o}_N(t_N) \hat{O}_N^\dagger \cdots \hat{O}_1^\dagger | \Psi_0 \rangle | \emptyset \rangle \langle \emptyset | \langle \Psi_0 | \hat{O}_1 \cdots \hat{O}_N \hat{o}_N^\dagger(t_N) \cdots \hat{o}_1^\dagger(t_1) | \Psi_0 \rangle | \emptyset \rangle \right\}$$

$$= \frac{1}{4}\text{Tr}_{\text{photons}}\left\{ \int_0^\infty dt_1 \cdots \int_0^\infty dt_N \langle \emptyset | \left[\prod_{j=1}^N \hat{a}_{e,j}(t_j)(\sqrt{p_\parallel}\hat{A}_{e,j}^\dagger + \sqrt{p_\perp' p_\perp}\hat{A}_{e'j}^\dagger \hat{L}_j^\dagger) + p_\parallel^{N/2}\prod_{j=1}^N \hat{a}_{l,j}(t_j)\hat{A}_{l,j}^\dagger \right. \right.$$

$$\left. + \sqrt{p_\perp' p_\parallel}p_\parallel^{(N-1)/2}\prod_{j=1}^N \hat{a}_{l,j}(t_j)\hat{A}_{l,j}^\dagger \hat{E}_j^\dagger \right] | \emptyset \rangle \langle \emptyset | \left[\prod_{i=1}^N \hat{a}_{e,i}(t_i)(\sqrt{p_\parallel}\hat{A}_{e,i}^\dagger + \sqrt{p_\perp' p_\perp}\hat{A}_{e'i}^\dagger \hat{L}_i^\dagger) \right.$$

$$\left. \left. + p_\parallel^{N/2}\prod_{i=1}^N \hat{a}_{l,i}(t_i)\hat{A}_{l,i}^\dagger + \sqrt{p_\perp' p_\parallel}p_\parallel^{(N-1)/2}\prod_{i=1}^N \hat{a}_{l,i}(t_i)\hat{A}_{l,i}^\dagger \hat{E}_i^\dagger \right]^\dagger | \emptyset \rangle \right\}$$

$$= \frac{1}{4}\text{Tr}_{\text{photons}}\left\{ \prod_{j=1}^N \int_0^\infty dt_j \langle \emptyset | \hat{a}_{e,j}(t_j)(\sqrt{p_\parallel}\hat{A}_{e,j}^\dagger + \sqrt{p_\perp' p_\perp}\hat{A}_{e'j}^\dagger \hat{L}_j^\dagger) | \emptyset \rangle \langle \emptyset | (\sqrt{p_\parallel}\hat{A}_{e,j} + \sqrt{p_\perp' p_\perp}\hat{A}_{e'j}\hat{L}_j)\hat{a}_{e,j}^\dagger(t_j) | \emptyset \rangle \right.$$

$$+ \frac{p_\parallel^N}{4}\prod_{j=1}^N \int_0^\infty dt_j \langle \emptyset | \hat{a}_{l,j}(t_j)\hat{A}_{l,j}^\dagger | \emptyset \rangle \langle \emptyset | \hat{A}_{l,j}\hat{a}_{l,j}^\dagger(t_j) | \emptyset \rangle + \frac{p_\parallel^N p_\perp'}{4}\prod_{j=1}^N \int_0^\infty dt_j \langle \emptyset | \hat{a}_{l,j}(t_j)\hat{A}_{l,j}^\dagger | \emptyset \rangle \langle \emptyset | \hat{A}_{l,j}\hat{a}_{l,j}^\dagger(t_j) | \emptyset \rangle$$

$$\left. + \frac{p_\parallel^{N/2}}{4}\left[\prod_{j=1}^N \int_0^\infty dt_j \langle \emptyset | \hat{a}_{e,j}(t_j)(\sqrt{p_\parallel}\hat{A}_{e,j}^\dagger + \sqrt{p_\perp' p_\perp}\hat{A}_{e'j}^\dagger \hat{L}_j^\dagger) | \emptyset \rangle \langle \emptyset | \hat{A}_{l,j}\hat{a}_{l,j}^\dagger(t_j) | \emptyset \rangle + \text{H.c.} \right] \right\}$$

$$= \frac{(p_\parallel + p_\perp' p_\perp)^N + p_\parallel^N(3 + p_\perp')}{4}. $$

2. Cluster state with branching error

A single round of the cluster-state preparation protocol in the presence of imperfect branching updates the state according to Eq. (55):

$$\hat{O}_j^\dagger = |+\rangle \langle 1| (\sqrt{p_\parallel}\hat{A}_{e,j}^\dagger + \sqrt{p_\perp' p_\perp}\hat{A}_{e',j}^\dagger \hat{L}_j^\dagger) + |-\rangle \langle 0| \sqrt{p_\parallel}\hat{A}_{l,j}^\dagger + |-\rangle \langle 1| \sqrt{p_\perp' p_\parallel}\hat{A}_{l,j}^\dagger \hat{E}_j^\dagger. \tag{D1}$$

The last term in the equation above gives a nonzero contribution to the fidelity only when the first photon is generated. To calculate the fidelity, we first ignore this term. The operator $\hat{o}(t_1)\hat{O}^\dagger$ in Eq. (10) corresponding to as single-photon state reads

$$\hat{o}_1(t_1)\hat{O}_1^\dagger = \sqrt{p_\parallel}(|1\rangle \langle 1| \hat{a}_{e,1}(t)\hat{A}_{e,1}^\dagger + |0\rangle \langle 0| \hat{a}_{l,1}(t)\hat{A}_{l,1}^\dagger) + \sqrt{p_\perp p_\perp'} |1\rangle \langle 1| \hat{a}_{e,1}(t)\hat{A}_{e',1}^\dagger \hat{L}_1^\dagger. \tag{D2}$$

The corresponding fidelity reads

$$\mathcal{F}^{(1)} = \int_0^\infty dt_1 \text{Tr}_{\text{photons}}\{ \langle \Psi_0 | \hat{o}_1(t_1)\hat{O}_1^\dagger | \Psi_0 \rangle \langle \emptyset | \langle \emptyset | \langle \Psi_0 | \hat{O}_1 \hat{o}_1^\dagger(t_1) \langle \Psi_0 | \} = p_\parallel + \frac{p_\perp' p_\perp}{4}. \tag{D3}$$

Analogously, for two photons,

$$\hat{o}_1(t_1)\hat{o}_2(t_2)\hat{O}_1^\dagger \hat{O}_2^\dagger = \frac{p_\parallel}{2}(|1\rangle \langle 1| \hat{a}_{e,1}(t)\hat{A}_{e,1}^\dagger + |0\rangle \langle 0| \hat{a}_{l,1}(t)\hat{A}_{l,1}^\dagger)(\hat{a}_{e,2}(t)\hat{A}_{e,2}^\dagger + \hat{a}_{l,2}(t)\hat{A}_{l,2}^\dagger)$$

$$+ \frac{\sqrt{p_\perp p'_\perp p_\parallel}}{2}[(\,|1\rangle\,\langle 1|\,\hat{a}_{e,1}(t)\hat{A}^\dagger_{e,1} + |0\rangle\,\langle 0|\,\hat{a}_{l,1}(t)\hat{A}^\dagger_{l,1})\hat{a}_{e',2}(t)\hat{A}^\dagger_{e',2}\hat{L}^\dagger_2$$

$$+ |1\rangle\,\langle 1|\,\hat{a}_{e,1}(t)\hat{A}^\dagger_{e,1}\hat{L}^\dagger_1(\hat{a}_{e,2}(t)\hat{A}^\dagger_{e,2} + \hat{a}_{l,2}(t)\hat{A}^\dagger_{l,2})] + \frac{p_\perp p'_\perp}{2}\,|1\rangle\,\langle 1|\,\hat{a}_{e,2}(t)\hat{A}^\dagger_{e,2}\hat{L}^\dagger_2\hat{a}_{e,1}(t)\hat{A}^\dagger_{e,1}\hat{L}^\dagger_1, \tag{D4}$$

and the corresponding fidelity is

$$\mathcal{F}^{(2)} = \int_0^\infty dt_2 \mathrm{Tr}_{\mathrm{photons}}\{\langle\Psi_0|\,\hat{o}_1(t_1)\hat{o}_2(t_2)\hat{O}^\dagger_2\hat{O}^\dagger_1\,|\Psi_0\rangle\,|\emptyset\rangle\,\langle\emptyset|\,\langle\Psi_0|\,\hat{O}_1\hat{O}_2\hat{o}^\dagger_2(t_2)\hat{o}^\dagger_1(t_1)\,|\Psi_0\rangle\} = \left(p_\parallel + \frac{p'_\perp p_\perp}{4}\right)^2. \tag{D5}$$

Repeating the same procedure N times, the N-photon unconditional fidelity reads

$$\mathcal{F}^{(N)} = \left(p_\parallel + \frac{p'_\perp p_\perp}{4}\right)^N. \tag{D6}$$

Finally, we multiply by the probability for the first photon to be emitted via the process described by the last term in Eq. (D1), which yields the total unconditional fidelity of the cluster state in the presence of imperfect branching (56),

$$\mathcal{F}^{(N)}[\mathrm{Cl}] = \left(p_\parallel + \frac{p_\perp p'_\perp}{4}\right)^{N-1}\left(p_\parallel + \frac{p_\perp p'_\perp}{4} + \frac{p_\parallel p'_\perp}{4}\right). \tag{D7}$$

APPENDIX E: BRANCHING ERROR DECOMPOSITION

As discussed in the main text dephasing and and excitation errors can be seen as single qubit errors affecting only a single photon. In this Appendix we analyze the nature of the branching errors, which flips the spin state. Since the spin acts as an entangler between subsequently emitted photons, errors in spin operation could potentially lead to delocalization of such errors between many photonic qubits. Below we show that this is not the case, and imperfect branching introduces only effective two-qubit errors between two subsequently emitted photons.

Consider all possible processes arising from branching errors. After a single round of the protocol, the state takes the form of Eq. (44), where all but two terms occur from various unwanted decay processes. For the realistic experimental parameters used in Fig. 8, only one of these processes occurs with a nonvanishing probability $P = p'_\perp p_\parallel$ and is described by an operator

$$\hat{\tilde{O}}^\dagger = \hat{R}\,|1\rangle\,\langle 1|\,\hat{A}^\dagger_{l,j}\hat{E}^\dagger_j. \tag{E1}$$

Here we choose $\hat{R} = \hat{H}$ that produces the cluster state, but the same analysis applies to the GHZ state. The remaining coefficients in Eq. (44) are at least two orders of magnitude smaller and such event therefore almost never appear in real situation. Ignoring these terms, we can represent a single repetition of the protocol with

$$\hat{\rho} \rightarrow p_\parallel \hat{O}^\dagger_{\mathrm{id}}\hat{\rho}\hat{O}_{\mathrm{id}} + p'_\perp p_\parallel \hat{\tilde{O}}^\dagger \hat{\rho}\hat{\tilde{O}} = p_\parallel \hat{O}^\dagger_{\mathrm{id}}\hat{\rho}\hat{O}_{\mathrm{id}} + p'_\perp p_\parallel \hat{\mathcal{E}}^\dagger \hat{O}^\dagger_{\mathrm{id}}\hat{\rho}\hat{O}_{\mathrm{id}}\hat{\mathcal{E}}, \tag{E2}$$

where $\hat{O}^\dagger_{\mathrm{id}}$ is the ideal operation of the protocol, $\hat{\tilde{O}}^\dagger$ is defined in Eq. (E1), and $\hat{\rho}$ is the systems density matrix. Hence, to prove that imperfect branching introduces at most two-photon errors, one needs to show that $\hat{\mathcal{E}}^\dagger$ is a two-qubit operator.

Consider two photons emitted in the ideal protocol, transforming the state according to

$$\hat{O}^\dagger_{\mathrm{id},j+1}\hat{O}^\dagger_{\mathrm{id},j} = |+\rangle\,a^\dagger_{e,j+1}(a^\dagger_{e,j}\,\langle 1| - a^\dagger_{l,j}\,\langle 0|) + |-\rangle\,a^\dagger_{l,j+1}(a^\dagger_{e,j}\,\langle 1| + a^\dagger_{l,j}\,\langle 0|). \tag{E3}$$

On the other hand, a photon emitted through the wrong process of Eq. (E1) followed by a correctly emitted photon corresponds to

$$\hat{O}^\dagger_{\mathrm{id},j+1}\hat{\tilde{O}}^\dagger_j = (\,|+\rangle\,\langle 1|\,a^\dagger_{e,j+1} + |-\rangle\,\langle 0|\,a^\dagger_{l,j+1})\,|-\rangle\,\langle 1|\,a^\dagger_{l,j} = |-\rangle\,\langle 1|\,a^\dagger_{l,j+1}a^\dagger_{l,j} - |+\rangle\,\langle 1|\,a^\dagger_{e,j+1}a^\dagger_{l,j}. \tag{E4}$$

Comparing the two equations above, one can notice that

$$\hat{O}^\dagger_{\mathrm{id},j+1}\hat{\tilde{O}}^\dagger_j = -a^\dagger_{l,j}a_{e,j}\hat{Z}_{j+1}\hat{O}^\dagger_{\mathrm{id},j+1}\hat{O}^\dagger_{\mathrm{id},j}. \tag{E5}$$

Therefore, the spin-flip error of Eq. (E1) effectively applies a two-photon error between subsequently emitted photons j and $j+1$,

$$\hat{\mathcal{E}}^\dagger = -a^\dagger_{l,j}a_{e,j}\hat{Z}_{j+1}. \tag{E6}$$

This error simultaneously flips the phase of photon $j+1$ and replaces the early jth photon with the late photon. Any subsequent operations commute with this error term, since they affect only later photons. The final state of the protocol can thus be understand as an error affecting an ideal state after its preparation.

As was noted earlier, for realistic experimental parameters used in this paper, any error other that (E1) occurs with a vanishingly small probability. Hence, incorrect branching operation always applies a two qubit error $\hat{\mathcal{E}}$, which according to Fig. 7 is 0.3%.

[1] P. Kok, W. J. Munro, K. Nemoto, T. C. Ralph, J. P. Dowling, and G. J. Milburn, Rev. Mod. Phys. **79**, 135 (2007).

[2] M. A. Nielsen, Phys. Rev. Lett. **93**, 040503 (2004).

[3] D. E. Browne and T. Rudolph, Phys. Rev. Lett. **95**, 010501 (2005).

[4] E. Knill, R. Laflamme, and G. J. Milburn, Nature (London) **409**, 46 (2001).

[5] K. Azuma, K. Tamaki, and H.-K. Lo, Nat. Commun. **6**, 6787 (2015).

[6] Z.-D. Li, R. Zhang, X.-F. Yin, L.-Z. Liu, Y. Hu, Y.-Q. Fang, Y.-Y. Fei, X. Jiang, J. Zhang, L. Li, N.-L. Liu, F. Xu, Y.-A. Chen, and J.-W. Pan, Nat. Photon. **13**, 644 (2019).

[7] D. Buterakos, E. Barnes, and S. E. Economou, Phys. Rev. X **7**, 041023 (2017).

[8] J. Borregaard, H. Pichler, T. Schröder, M. D. Lukin, P. Lodahl, and A. S. Sørensen, Phys. Rev. X **10**, 021071 (2020).

[9] P. Hilaire, E. Barnes, and S. E. Economou, Quantum **5**, 397 (2021).

[10] J.-W. Pan, D. Bouwmeester, M. Daniell, H. Weinfurter, and A. Zeilinger, Nature (London) **403**, 515 (2000).

[11] H.-X. Lu, L.-Z. Cao, J.-Q. Zhao, Y.-D. Li, and X.-Q. Wang, Sci. Rep. **4**, 4476 (2014).

[12] M. Żukowski, Phys. Rev. A **61**, 022109 (2000).

[13] D. C. Burnham and D. L. Weinberg, Phys. Rev. Lett. **25**, 84 (1970).

[14] P. G. Kwiat, K. Mattle, H. Weinfurter, A. Zeilinger, A. V. Sergienko, and Y. Shih, Phys. Rev. Lett. **75**, 4337 (1995).

[15] A. G. White, D. F. V. James, P. H. Eberhard, and P. G. Kwiat, Phys. Rev. Lett. **83**, 3103 (1999).

[16] D. Bouwmeester, J.-W. Pan, M. Daniell, H. Weinfurter, and A. Zeilinger, Phys. Rev. Lett. **82**, 1345 (1999).

[17] A.-N. Zhang, C.-Y. Lu, X.-Q. Zhou, Y.-A. Chen, Z. Zhao, T. Yang, and J.-W. Pan, Phys. Rev. A **73**, 022330 (2006).

[18] A. Zeilinger, M. A. Horne, H. Weinfurter, and M. Żukowski, Phys. Rev. Lett. **78**, 3031 (1997).

[19] C.-Y. Lu, X.-Q. Zhou, O. Gühne, W.-B. Gao, J. Zhang, Z.-S. Yuan, A. Goebel, T. Yang, and J.-W. Pan, Nat. Phys. **3**, 91 (2007).

[20] X.-C. Yao, T.-X. Wang, P. Xu, H. Lu, G.-S. Pan, X.-H. Bao, C.-Z. Peng, C.-Y. Lu, Y.-A. Chen, and J.-W. Pan, Nat. Photon. **6**, 225 (2012).

[21] X.-L. Wang, L.-K. Chen, W. Li, H.-L. Huang, C. Liu, C. Chen, Y.-H. Luo, Z.-E. Su, D. Wu, Z.-D. Li, H. Lu, Y. Hu, X. Jiang, C.-Z. Peng, L. Li, N.-L. Liu, Y.-A. Chen, C.-Y. Lu, and J.-W. Pan, Phys. Rev. Lett. **117**, 210502 (2016).

[22] H.-S. Zhong, Y. Li, W. Li, L.-C. Peng, Z.-E. Su, Y. Hu, Y.-M. He, X. Ding, W. Zhang, H. Li, L. Zhang, Z. Wang, L. You, X.-L. Wang, X. Jiang, L. Li, Y.-A. Chen, N.-L. Liu, C.-Y. Lu, and J.-W. Pan, Phys. Rev. Lett. **121**, 250505 (2018).

[23] K. M. Gheri, C. Saavedra, P. Törmä, J. I. Cirac, and P. Zoller, Phys. Rev. A **58**, R2627 (1998).

[24] C. Saavedra, K. M. Gheri, P. Törmä, J. I. Cirac, and P. Zoller, Phys. Rev. A **61**, 062311 (2000).

[25] C. Schön, E. Solano, F. Verstraete, J. I. Cirac, and M. M. Wolf, Phys. Rev. Lett. **95**, 110503 (2005).

[26] N. H. Lindner and T. Rudolph, Phys. Rev. Lett. **103**, 113602 (2009).

[27] J. P. Lee, B. Villa, A. J. Bennett, R. M. Stevenson, D. J. P. Ellis, I. Farrer, D. A. Ritchie, and A. J. Shields, Quantum Sci. Technol. **4**, 025011 (2019).

[28] I. Schwartz, D. Cogan, E. R. Schmidgall, Y. Don, L. Gantz, O. Kenneth, N. H. Lindner, and D. Gershoni, Science **354**, 434 (2016).

[29] R. Vasconcelos, S. Reisenbauer, C. Salter, G. Wachter, D. Wirtitsch, J. Schmiedmayer, P. Walther, and M. Trupke, npj Quantum Inf. **6**, 9 (2020).

[30] M. Hillery, V. Bužek, and A. Berthiaume, Phys. Rev. A **59**, 1829 (1999).

[31] S. E. Economou, N. Lindner, and T. Rudolph, Phys. Rev. Lett. **105**, 093601 (2010).

[32] M. Gimeno-Segovia, T. Rudolph, and S. E. Economou, Phys. Rev. Lett. **123**, 070501 (2019).

[33] H. A. Zaidi, C. Dawson, P. van Loock, and T. Rudolph, Phys. Rev. A **91**, 042301 (2015).

[34] M. Keller, B. Lange, K. Hayasaka, W. Lange, and H. Walther, Nature (London) **431**, 1075 (2004).

[35] H. G. Barros, A. Stute, T. E. Northup, C. Russo, P. O. Schmidt, and R. Blatt, New J. Phys. **11**, 103004 (2009).

[36] T. Walker, K. Miyanishi, R. Ikuta, H. Takahashi, S. Vartabi Kashanian, Y. Tsujimoto, K. Hayasaka, T. Yamamoto, N. Imoto, and M. Keller, Phys. Rev. Lett. **120**, 203601 (2018).

[37] N. Mizuochi, T. Makino, H. Kato, D. Takeuchi, M. Ogura, H. Okushi, M. Nothaft, P. Neumann, A. Gali, F. Jelezko, J. Wrachtrup, and S. Yamasaki, Nat. Photon. **6**, 299 (2012).

[38] I. Aharonovich, S. Castelletto, D. A. Simpson, C.-H. Su, A. D. Greentree, and S. Prawer, Rep. Prog. Phys. **74**, 076501 (2011).

[39] M. Gimeno-Segovia, P. Shadbolt, D. E. Browne, and T. Rudolph, Phys. Rev. Lett. **115**, 020502 (2015).

[40] C. T. Nguyen, D. D. Sukachev, M. K. Bhaskar, B. Machielse, D. S. Levonian, E. N. Knall, P. Stroganov, R. Riedinger, H. Park, M. Lončar, and M. D. Lukin, Phys. Rev. Lett. **123**, 183602 (2019).

[41] M. K. Bhaskar, R. Riedinger, B. Machielse, D. S. Levonian, C. T. Nguyen, E. N. Knall, H. Park, D. Englund, M. Lončar, D. D. Sukachev, and M. D. Lukin, Nature (London) **580**, 60 (2020).

[42] P. Glasenapp, D. S. Smirnov, A. Greilich, J. Hackmann, M. M. Glazov, F. B. Anders, and M. Bayer, Phys. Rev. B **93**, 205429 (2016).

[43] S. Das, L. Zhai, M. Čepulskovskis, A. Javadi, S. Mahmoodian, P. Lodahl, and A. S. Sørensen, arXiv:1912.08303.

[44] E. L. Hahn, Phys. Rev. **80**, 580 (1950).

[45] F. H. L. Koppens, K. C. Nowack, and L. M. K. Vandersypen, Phys. Rev. Lett. **100**, 236802 (2008).

[46] X. J. Wang, S. Chesi, and W. A. Coish, Phys. Rev. Lett. **109**, 237601 (2012).

[47] L. Huthmacher, R. Stockill, E. Clarke, M. Hugues, C. Le Gall, and M. Atatüre, Phys. Rev. B **97**, 241413(R) (2018).

[48] D. Press, K. De Greve, P. L. McMahon, T. D. Ladd, B. Friess, C. Schneider, M. Kamp, S. Höfling, A. Forchel, and Y. Yamamoto, Nat. Photon. **4**, 367 (2010).

[49] M. Lauritzen, Spin-photon entanglement realised by quantum dots embedded in waveguides, Master's thesis, University of Copenhagen (2019).

[50] P. Lodahl, S. Mahmoodian, and S. Stobbe, Rev. Mod. Phys. **87**, 347 (2015).

[51] P. L. Mirambell, Fidelity characterization of spin-photon entangled states, Master's thesis, University of Copenhagen (2019).

[52] K. Tiurev, M. H. Appel, P. L. Mirambell, M. B. Lauritzen, A. Tiranov, P. Lodahl, and A. S. Sørensen, arXiv:2007.09295.

[53] R. Raussendorf, J. Harrington, and K. Goyal, New J. Phys. **9**, 199 (2007).

[54] R. Raussendorf and J. Harrington, Phys. Rev. Lett. **98**, 190504 (2007).

[55] R. Raussendorf, J. Harrington, and K. Goyal, Ann. Phys. **321**, 2242 (2006).

[56] I. Aharonovich, D. Englund, and M. Toth, Nat. Photon. **10**, 631 (2016).

[57] M. Atatüre, D. Englund, N. Vamivakas, S.-Y. Lee, and J. Wrachtrup, Nat. Rev. Mater. **3**, 38 (2018).

[58] D. D. Awschalom, R. Hanson, J. Wrachtrup, and B. B. Zhou, Nat. Photon. **12**, 516 (2018).

[59] J. H. Bodey, R. Stockill, E. V. Denning, D. A. Gangloff, G. Éthier-Majcher, D. M. Jackson, E. Clarke, M. Hugues, C. L. Gall, and M. Atatüre, npj Quantum Inf. **5**, 95 (2019).

[60] M. Arcari, I. Söllner, A. Javadi, S. Lindskov Hansen, S. Mahmoodian, J. Liu, H. Thyrrestrup, E. H. Lee, J. D. Song, S. Stobbe, and P. Lodahl, Phys. Rev. Lett. **113**, 093603 (2014).

[61] V. Lipinska, G. Murta, and S. Wehner, Phys. Rev. A **98**, 052320 (2018).

[62] M. Christandl and S. Wehner, in *Advances in Cryptology: ASIACRYPT 2005*, edited by B. Roy (Springer, Berlin, 2005), pp. 217–235.

[63] G. Brassard, A. Broadbent, J. Fitzsimons, S. Gambs, and A. Tapp, in *Advances in Cryptology: ASIACRYPT 2007*, edited by K. Kurosawa (Springer, Berlin, 2007), pp. 460–473.

[64] E. D'Hondt and P. Panangaden, Quantum Inf. Comput. **6**, 173 (2006).